processes

MDPI

Article

Evaluation of the Hydraulic Fracturing Tendencies of Consolidated Sandstone Reservoirs Based on the Catastrophe Theory

Haowei Feng [1,2,*], Ping Wang [1,2], Zhan Qu [1,2], Hai Huang [1,2], Liang Wang [1,2], Yongsheng Wei [1,2] and Yawen He [3]

[1] School of Petroleum Engineering, Xi'an Shiyou University, Xi'an 710065, China; wp8230@xsyu.edu.cn (P.W.); zhqu@xsyu.edu.cn (Z.Q.); huanghai@xsyu.edu.cn (H.H.); wangliang@xsyu.edu.cn (L.W.); 13659969371@163.com (Y.W.)
[2] Key Laboratory of Oil and Gas Well and Reservoir Permeability and Rock Mechanics in Shaanxi Province, Xi'an 710065, China
[3] Yumen Drilling Company, Western Drilling Corporation, Jiuquan 735000, China; gh220717@163.com
* Correspondence: 15595401668@163.com

Abstract: The evaluation of rock hydraulic fracturing tendency plays a crucial role in the selection of fracturing layers within reservoirs and the evaluation of post-compression capacity. The sandstone reservoirs in the Yihuang New Area have poor physical properties and are deeply buried. It is necessary to increase the production of oil and gas by hydraulic fracturing. Regarding the sandstones in the region, the following parameters were considered: combined compressive strength, bulk modulus, shear modulus, fracture index, horizontal-stress difference coefficient, and fracture toughness. In accordance with the catastrophe theory, a multi-level structure was established for the hydraulic fracturing-tendency evaluation of sandstone reservoirs, consisting of a target layer, a guide layer, and an indicator layer. A catastrophic model for evaluating the hydraulic fracturing tendency of sandstone reservoirs was established. The results are consistent with those obtained from the Analytic Hierarchy Process. However, the catastrophe theory significantly reduces subjective interference. The results indicate that when the hydraulic fracturing-tendency evaluation value is greater than 0.8, the reservoir can be fractured well; when the hydraulic fracturing-tendency evaluation value is between 0.7 and 0.8, the fracture reservoir is moderate; and when the hydraulic fracturing-tendency evaluation value is less than 0.7, the fractured reservoir is poor. The optimal fracture intervals for the Yi 70 well are 1320–1323 m, 1350–1355 m, and 1355–1360 m. The optimal fracture planes for the Yi 76 well are 1921–1925 m and 1925–1930 m. The optimal fracture planes for the Yi 10-1-26 well are 2487–2495 m, 2585–2587 m, and 2589–2591 m. The hydraulic fracturing-tendency model developed in this study has been applied to several well sections of sandstone reservoirs in the Yihuang New Area. Additionally, the model was compared with existing hydraulic fracturing-tendency evaluation models. The evaluation results are in agreement with the post-pressure capacity-monitoring data. The accuracy of the model presented in this study has been verified, as has its applicability to other sandstone reservoirs.

Keywords: catastrophe theory; hydraulic fracturing-tendency evaluation; sandstone reservoir; rock mechanics properties

Citation: Feng, H.; Wang, P.; Qu, Z.; Huang, H.; Wang, L.; Wei, Y.; He, Y. Evaluation of the Hydraulic Fracturing Tendencies of Consolidated Sandstone Reservoirs Based on the Catastrophe Theory. *Processes* **2024**, *12*, 1439. https://doi.org/10.3390/pr12071439

Academic Editors: Jan Vinogradov and Ali Habibi

Received: 21 May 2024
Revised: 28 June 2024
Accepted: 8 July 2024
Published: 10 July 2024

1. Introduction

Hydraulic fracturing technology is of significant importance in the context of oil and gas extraction. It can effectively increase oil and gas production, extend production cycles, and enhance recovery rates. It expands the range of recoverable reserves. It is of great importance for the effective development and utilization of oil and gas resources [1–3]. The term "reservoir hydraulic fracturing tendency" refers to the capacity of reservoir rock to be effectively fractured and form efficient fractures during the hydraulic fracturing process.

The evaluation of reservoir hydraulic fracturing tendency is an important basis for selecting layers for reservoir fracturing and determining fracturing program design [4,5].

Reservoir hydraulic fracturing tendency is typically assessed using the rock brittleness index. It has been demonstrated that higher brittleness and brittleness indexes correspond to easier reservoir fracturing and relatively higher production capacity. The brittleness index represents a convenient and straightforward method for evaluating reservoir hydraulic fracturing tendency. Nevertheless, the sole reliance on the brittleness index for the evaluation of reservoir hydraulic fracturing tendency may result in unreliability or even inaccuracy. The brittleness index is not an accurate reflection of the ease of reservoir fracturing. It is possible for a reservoir to exhibit a high brittleness index yet be difficult to fracture during actual operations. Consequently, a reliable and accurate evaluation of reservoir hydraulic fracturing tendency based solely on the brittleness index is not possible [6–9]. In a pioneering study, Junliang Yuan and colleagues [10] integrated the brittleness index with fracture toughness in a novel manner. In the development of a hydraulic fracturing tendency model for unconventional reservoirs, Guozhang Zhu et al. [11] proposed a method for evaluating the hydraulic fracturing tendency logging of deep shale formations by integrating the mechanical brittleness and fracture toughness of the formation rock. The evaluation of shale gas reservoirs was conducted in an efficient manner under high-temperature and high-pressure conditions. In their study, Cheng Chen and colleagues [12] examined the relationship between reservoir characteristics and the brittleness index, as well as elastomechanical parameters. The researchers put forth the suggestion that several additional parameters be incorporated into the comprehensive hydraulic fracturing tendency evaluation of reservoirs, including the natural fracture development index, permeability inhomogeneity, and the degree of original pressure retention. Jinzhou Zhao and colleagues [13] developed a method for evaluating the hydraulic fracturing tendency of shale based on three key characteristics: brittleness, fracture toughness, and natural fractures. In their study, Jianfeng Xiao and colleagues [14] considered three perspectives: mineral composition, tensile–compressive strength ratio, and coefficient of horizontal stress difference. The objective of this study was to evaluate hydraulic fracturing tendency in the Weiyuan area. In their investigation, Yonghao Zhang et al. [15] initially examined the complexity of rock core rupture under pressure. Subsequently, they developed a set of tests and analytical methods to assess core hydraulic fracturing tendency. In a study published in 2016, Junbin Chen and colleagues [16] synthesized the mineral composition and microscopic mechanical parameters. The utilization of normalization, harmonic mean, arithmetic mean, and other statistical techniques was employed in order to facilitate the analysis of the data. A quantitative assessment of the hydraulic fracturing tendency of various types of shale gas was conducted. In their study, Liang Wang and colleagues [17] employed a multifactorial approach, considering brittleness, fracture toughness, the horizontal stress difference coefficient, and the impact index of natural fractures. Through the establishment of a hydraulic fracturing tendency evaluation method for shale oil reservoirs in the Duanzhai section of the central Sichuan region, Jianmeng Sun et al. [18] investigated the logging evaluation of hydraulic fracturing tendency in tight gas reservoirs, focusing on two perspectives: the brittleness index of tight sandstones and fracture toughness. In their study, Chong Zhang and colleagues [19] employed the Analytic Hierarchy Process to consider a range of factors, including the brittleness index, interlayer occlusion effect, natural fracture development index, horizontal stress difference, and fracture toughness. A method for evaluating the hydraulic fracturing tendency of sandstone reservoirs was established. The majority of the aforementioned hydraulic fracturing tendency evaluation methods employ the Analytic Hierarchy Process, which inherently introduces a degree of subjectivity. In order to significantly reduce the impact of subjective factors, catastrophe theory is incorporated into the hydraulic fracturing-tendency evaluation method. In a study published in 2018, Li Jun [20] and colleagues employed catastrophe theory to investigate the influence of the shale brittleness index, mineral composition, gas content, fracture toughness, and other factors on hydraulic fracturing tendency. A model was developed to

evaluate the hydraulic fracturing tendency of shale reservoirs with extended horizontal wellbore sections. A novel approach to evaluating the hydraulic fracturing tendency of shale reservoirs was presented. Ren Lan [21] and others employed catastrophe theory to synthesize shale reservoir geology, the degree of seam network development, rock matrix, fluid usage, construction parameters, and other characteristics. This synthesis was used to develop an integrated geological–engineering hydraulic fracturing-tendency method to predict the economic benefits of fracturing. At present, the application of catastrophe theory to the evaluation of the compressibility of sandstone reservoirs is limited.

Through research and analysis, it is evident that previous scientists have encountered the following problems in their research on reservoir hydraulic fracturing-tendency evaluation: (1) a significant number of researchers have conducted comprehensive studies on the evaluation of hydraulic fracturing tendency in shale oil and gas reservoirs. Nevertheless, research on the hydraulic fracturing tendency of sandstone reservoirs remains limited. A lack of both harmonized standards and a set of reliable and effective methods persist. (2) A substantial number of hydraulic fracturing-tendency evaluation methods fail to provide a comprehensive consideration of mechanical parameters. Only those mechanical parameters that are commonly used are considered, and the effects of shear modulus and bulk modulus on hydraulic fracturing tendency are ignored. (3) The majority of existing hydraulic fracturing-tendency evaluation methods utilize the Analytic Hierarchy Process. The requirement for human determination of parameter weights does not eliminate human subjectivity. The reliability and accuracy of the method in question have been the subject of considerable debate, with the result that the conclusions of the hydraulic fracturing-tendency evaluation are open to question.

In light of the aforementioned considerations, this paper makes the following contributions: (1) incorporating catastrophe theory into methods for evaluating sandstone reservoir hydraulic fracturing tendency. Catastrophe theory is applicable to systems where the internal roles are not yet known with certainty. One advantage of this approach is that it does not require the artificial determination of the weights for each parameter. Furthermore, it significantly reduces subjective interference compared to the commonly employed Analytic Hierarchy Process. (2) The integration of indoor core tests with well logging data led to the generation of more precise mechanical parameters for each well section. (3) A comprehensive analysis was conducted on the rocks, including compressive strength, shear modulus, bulk modulus, rock brittleness, horizontal stress difference coefficient, and fracture toughness. A method for evaluating the hydraulic fracturing tendency of sandstone reservoirs in the Yihuang New Area based on catastrophe theory is proposed. A comparison can be made between this method and the widely used Analytic Hierarchy Process, with the objective of enhancing the accuracy of evaluating sandstone reservoir hydraulic fracturing tendency. The objective is to enhance the outcomes of fracking operations and provide effective guidance for field fracking activities.

2. Geological Background

The Yihuang New District is situated in Yichuan County, Shaanxi Province, in the outer region of the Weibei Uplift Zone within the Ordos Basin. Yichuan County is situated at the intersection of the Qinling Orogeny and the North China Craton in China. The region's geology is characterized by a complex structural framework, predominantly shaped by the Qinling Mountains and the surrounding alluvial plains.

The rock formations in Yihuang New District are diverse and complex. The predominant rock types include gneiss, graystone, sandstone, shale, coal, and others. Sandstones and shales are primarily located in the alluvial plain regions. The sandstone formations in the Ordos Basin serve as an important reservoir, particularly the dense sandstone layers. Typically, these tight sandstones exhibit low porosity and permeability. Nevertheless, the application of technology, such as horizontal drilling and hydraulic fracturing, can enhance the capacity for production.

This paper examines the hydraulic fracturing tendency of reservoirs in select well sections of Yichuan gas wells. The depth of the reservoirs in the selected gas wells ranges from approximately 1286 m to 2591 m. Figure 1a presents a comprehensive logging interpretation map of section 1 of the Shanxi Formation at the Yi70 well, situated in the southeastern Ordos Basin. The data indicate that sandstone is well-developed while mudstone is limited in the sections at 1320–1323 m, 1350–1355 m, and 1355–1360 m in the Yi70 well. Figure 1b presents a comprehensive diagram that illustrates the logging interpretation of the Taiyuan and Shanxi formations for the Yi10-1-26 well. The well displays the presence of developed sandstone and undeveloped mudstone within the specified intervals, namely 2487–2495 m, 2503–2512 m, 2585–2587 m, and 2589–2591 m. Figure 1c presents a comprehensive map that illustrates the logging interpretation of the Box 8 Formation and the Shanxi Formation 1 section. This section is located within the Yi76 well, situated within the northeastern Ordos Basin. The data indicate that the well exhibits sandstone development and mudstone underdevelopment within the intervals at 1870–1875 m, 1921–1925 m, and 1925–1930 m.

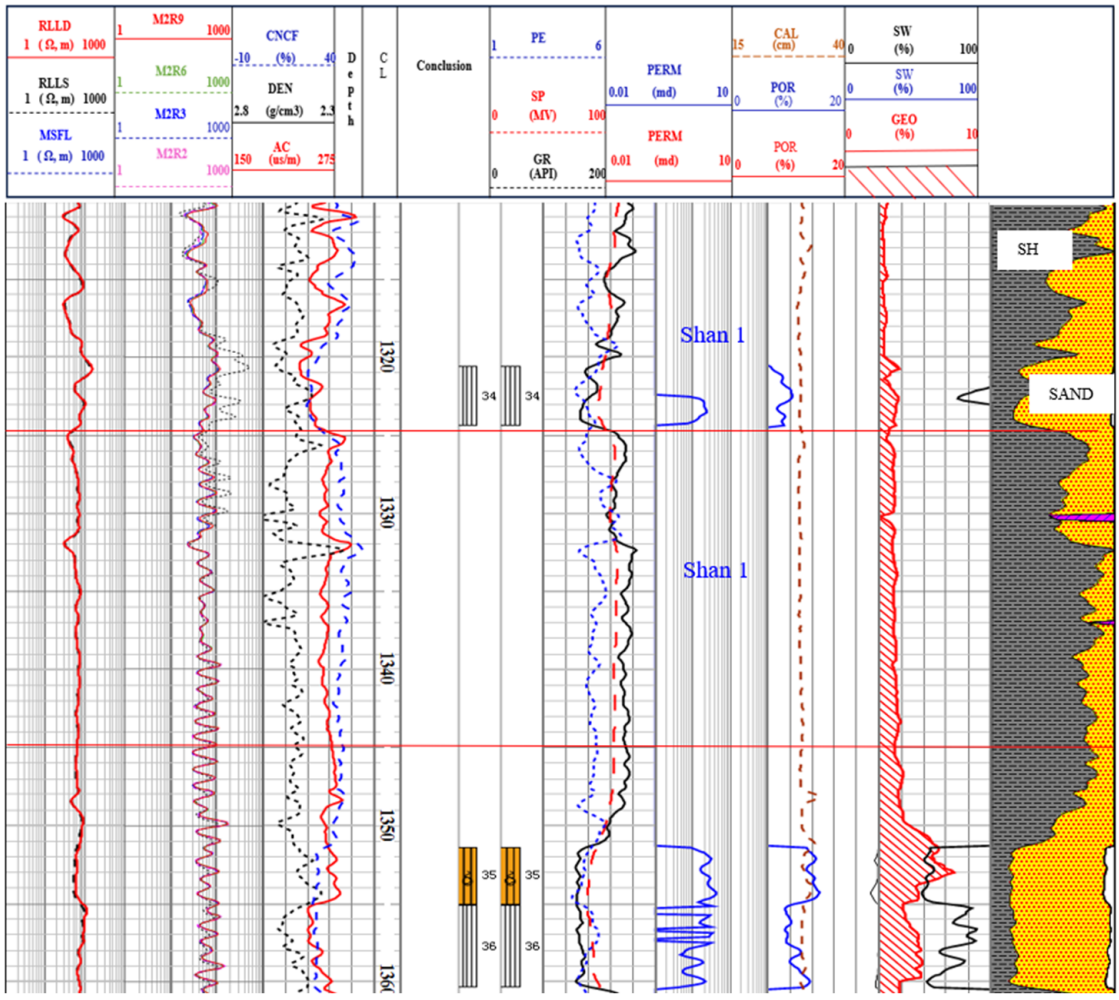

(**a**)

Figure 1. *Cont.*

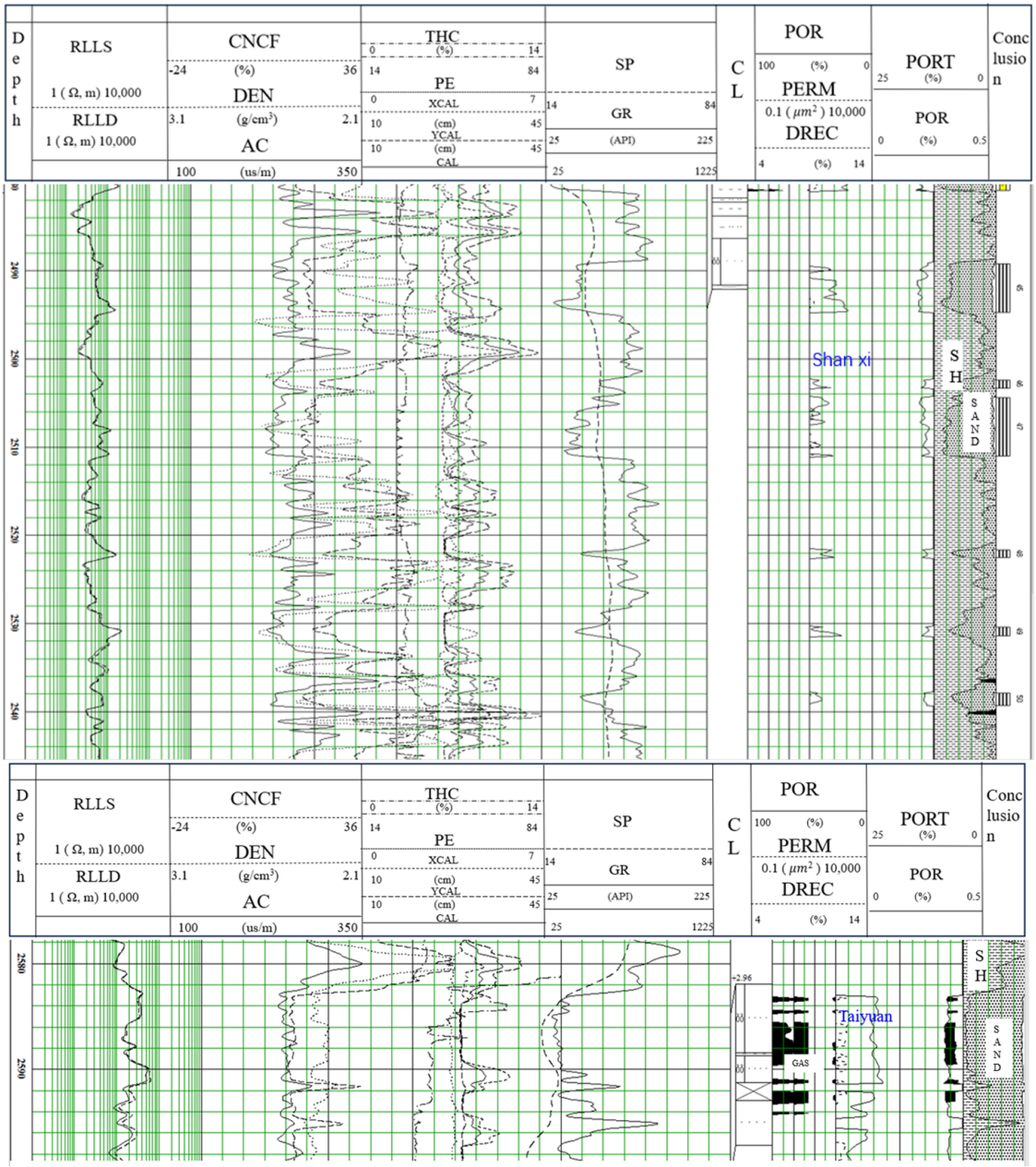

(**b**)

Figure 1. *Cont*.

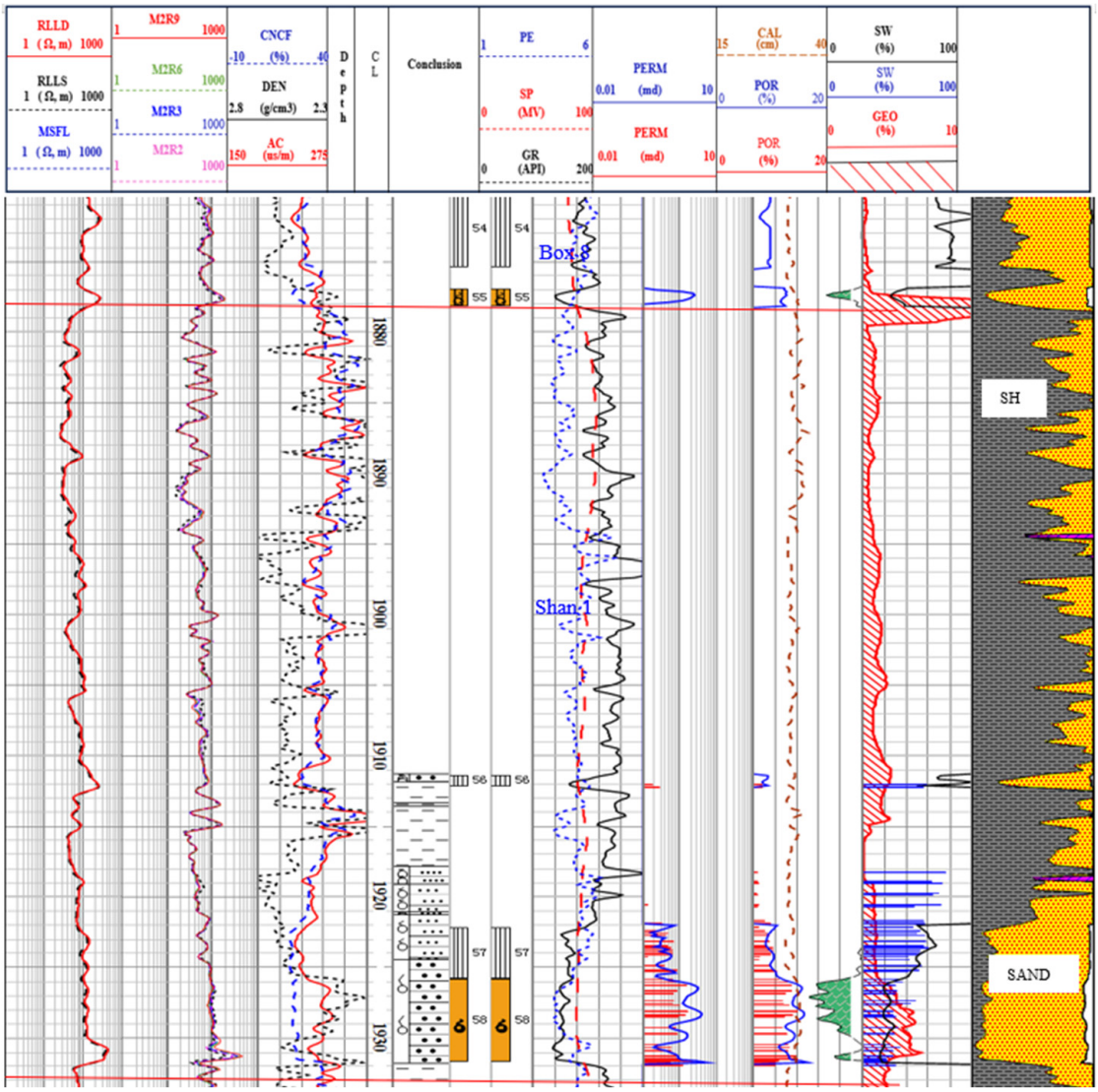

(**c**)

Figure 1. Logging Curves for Various Wells. (**a**) Comprehensive interpretation of logging data from the Yi 70 Well; (**b**) Comprehensive interpretation of logging data from the Yi 10-1-26 Well; (**c**) Comprehensive interpretation of Logging Data from the Yi 76 Well.

The logging-interpretation synthesized map indicates that the average porosity of the Shanxi Formation 1 section of the Yi70 well is approximately 3.2%, 7.6%, and 5.9% at depths of 1320–1323 m, 1350–1355 m, and 1355–1360 m, respectively, while the average permeability is approximately 0.037 mD, 0.084 mD, and 0.053 mD, respectively. The average porosity of the Taiyuan and Shanxi Formations in well Yi10-1-26 is approximately 5.2%, 3.7%, 6.96%, and 5.6% at depths of 2487–2495 m, 2503–2512 m, 2585–2587 m, and 2589–2591 m, respectively, while the average permeability is approximately 0.065 mD, 0.07 mD, 0.35 mD, and 0.13 mD. The average porosity of the Box 8 Group and Shanxi Group 1 sections of the Yi76 well at depths of 1870–1875 m, 1921–1925 m, and 1925–1930 m is approximately 3.3%, 2.3%, and 6.0%, respectively, while the average permeability is approximately 0.026 mD, 0.047 mD, and 0.097 mD, respectively.

3. Methodology

3.1. X-ray Diffraction Analysis

Following the grinding of the rock samples to a particle size of less than 1 mm, the clays were separated by centrifugation, and oriented flakes were prepared. XRD measurements were subsequently performed on a MinFlexII polycrystalline X-ray diffractometer (Bruker, Bremen, Germany). The basic framework diagram of the device, shown in Figure 2, includes an X-ray generator with a power of 3.5 kW. A ceramic X-ray tube with a power of 1.0 kW and a copper-target vertical goniometer (Q/2Q) with a goniometric accuracy of 0.0001 degrees were employed.

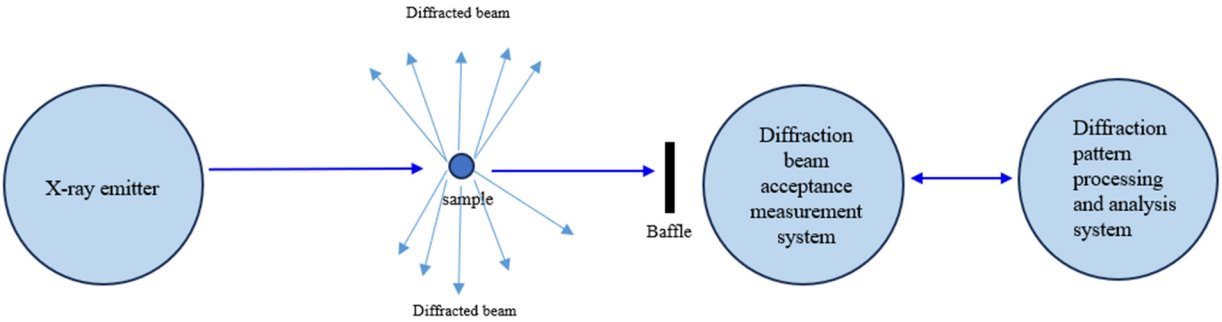

Figure 2. Basic framework diagram of the equipment.

Mineralogical analysis was conducted via X-ray diffraction. The results indicate that the mineralogical fractions of the sandstones in the region are predominantly clastic and quartz sandstones. The brittleness index of the rocks was determined using the mineral composition method.

3.2. Uniaxial Compression Experiment

Prior to the commencement of the experiment, it was necessary to standardize the cores in accordance with the standards set forth by the International Society of Rock Mechanics. The dimensions of the treated rock samples were 25 mm × 50 mm. Illustrations of standard rock samples are provided, and all processed rock samples are shown in Figure A1 of Appendix A. Subsequently, uniaxial compression tests were conducted utilizing the RTR-1000 Rock Mechanics Servo Test System (GCTS Testing Systems, Tempe, AZ, USA).

Mechanical parameters, including uniaxial compressive strength, elastic modulus, Poisson's ratio, shear modulus, and bulk modulus, were obtained through uniaxial compressive strength experiments. One such method is the elastodynamic parametric approach proposed by Rickman. The brittleness index of the rock can be determined using the elastic modulus and Poisson's ratio. Combining the mineral composition analysis method with the elastomechanical parametric methods allows for the determination of the brittleness index. A brittleness-index evaluation method was developed for the new Yihuang district in the study area. This method employs mechanical parameters, including compressive strength, brittleness index, shear modulus, and bulk modulus. The mechanical parameters of the entire well section can be determined through indoor core experiments combined with logging data.

3.3. Geostress Experiment

The objective is to ascertain the three principal geopathic stresses (one vertical, two horizontal) acting on the rock sample in the subsurface. This can be achieved through experimental means by taking the cores of rock samples in various directions. In practice, the overlying formation pressure can be accurately determined using density logging. Consequently, the Kaiser-effect experiment can be conducted by taking three small core samples spaced 45° apart in the horizontal direction, as illustrated in Figure 3. The experimental setup comprises a rock mechanics testing system and a PAC acoustic emission

testing system (Physical Acoustics Corp., West Windsor Township, NJ, USA), as illustrated in Figure 4. The rock mechanics testing system is responsible for applying the loads, while the acoustic emission testing system is tasked with collecting the acoustic emission signals generated within the core during the loading process. Based on the outcomes of this experiment, the maximum and minimum principal ground stresses applied to the specimen downhole can be determined using the corresponding equations. The horizontal-stress variance factor needs to be finalized.

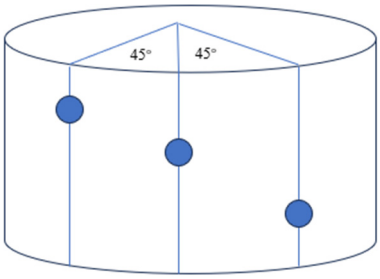

Figure 3. The schematic diagram of core sampling in the acoustic emitter experiment.

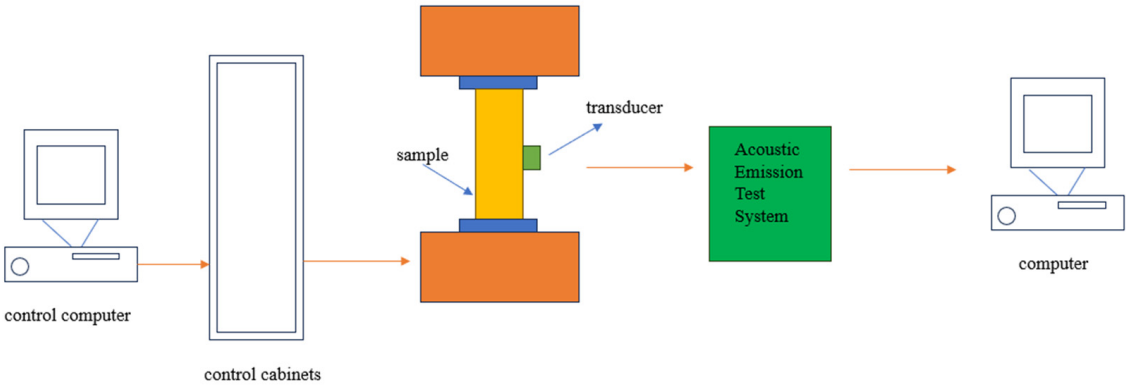

Figure 4. A block diagram of the rock acoustic-emission Kaiser-effect test system.

3.4. Hydraulic Fracturing-Tendency Catastrophe Modeling of Sandstone Reservoirs

Drawing on the fundamentals of catastrophe theory, sandstone reservoir hydraulic fracturing-tendency assessment (S) is taken as the target layer. The positive correlation indicator (A) and negative correlation indicator (B) are taken as the criterion layer. The brittleness index (A1) and shear modulus (A2) are taken as indicator layers for positive correlation indicators. Compressive strength (B1), horizontal-stress differential coefficient (B2), fracture toughness (B3), and bulk modulus (B4) were used as indicator layers for negative correlation indicators, as shown in Figure 5. The system is divided into subsystems, each containing multiple evaluation indicators. The type of catastrophe model for a subsystem must be determined based on its number of indicators. There are two groups of cusp catastrophes: (S, A, and B) and (A, A1, and A2). There is one group of butterfly catastrophes: (B, B1, B2, B3, and B4). The indicator layers (A1, A2, B1, B2, B3, and B4) of the sandstone reservoir were then made dimensionless. Calculations were performed for two sets of cusp catastrophes and one set of butterfly catastrophes using their respective catastrophe-model normalization formulas. Finally, the results of the sandstone reservoir hydraulic fracturing-tendency assessment (S) were obtained.

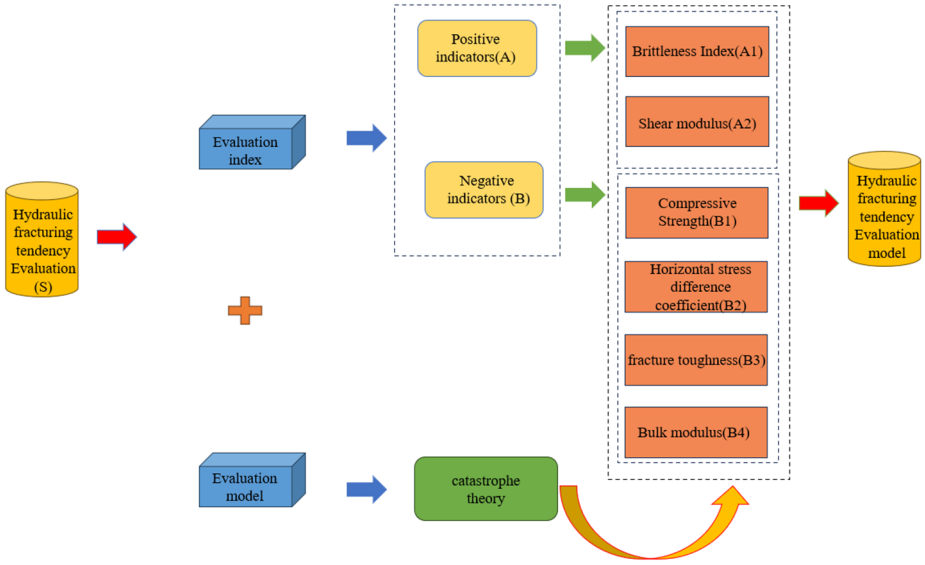

Figure 5. Flowchart for hydraulic fracturing-tendency evaluation.

4. Mechanical Experiments

4.1. Preparation of Rock Specimens

The research test samples were collected from the intervals at 1320–1323 m, 1350–1355 m, and 1355–1360 m in the Yi 70 well within this zone. The Yi 10-1-26 well was sampled at depths of 2487–2495 m, 2503–2512 m, 2585–2587 m, and 2589–2591 m. The Yi 76 well was sampled at depths of 1870–1875 m, 1921–1925 m, and 1925–1930 m. The low average porosity value in the previous section indicates that the reservoir rock has less pore space and a tighter structure, suggesting that the rock is more consolidated. A low mean permeability value indicates a highly consolidated rock with poor pore connectivity or very small pores. Taken together, the low porosity and permeability indicate a high degree of consolidation of the reservoir rock.

In accordance with the experimental protocol, three small cores were extracted in three directions, each separated by 45° horizontally, as illustrated in Figure 3. Representative examples of the processed specimens are illustrated in Figure 6.

Figure 6. Photos of some rock samples.

4.2. Device and Process for Uniaxial Compressive Strength Testing

The Rock Mechanics Servo Test System (RTR-1000) manufactured by GCTS (Tempe, AZ, USA) was used as shown in Figure 7. The uniaxial compression test was performed according to the following procedure: (1) the prepared specimen is aligned with the upper and lower compression plates. The specimen and plate are wrapped in a latex-based protective sleeve. The gasket is then fitted to seal the specimen and placed in the compression chamber. Ensure that the specimen axis is aligned with the loader axis. Ensure that the loading head of the instrument is in contact with the top surface of the specimen. (2) Apply vertical downward pressure until the specimen is crushed. (3) Record stress and deformation data during loading. If damage occurs, record the maximum load capacity and damage pattern.

Figure 7. Triaxial testing system by GCTS in the United States.

4.3. Specimen after Fracturing Rock

Figure 8 depicts the sandstone specimen following the uniaxial compressive strength test. The rock sample without the protective cover is shown below. The figure illustrates the formation of cracks on the specimen's surface, which has become rough. Some specimens exhibited dislodgment of particles adhering to the sample surface, with the particles breaking down along the cracks across a wide area. The high quartz content of the shale is responsible for the difficulty of the shale deforming plastically under pressure, which renders it prone to brittle rupture and crack formation.

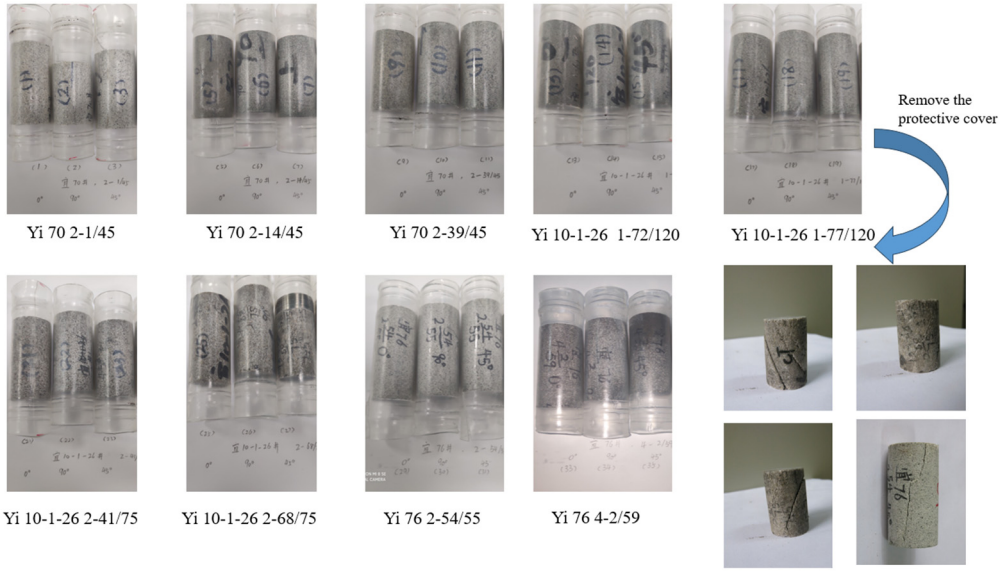

Figure 8. Rock specimen after fracturing.

5. Experimental Results Analysis

The mechanical parameters, including compressive strength, elastic modulus, Poisson's ratio, shear modulus, and bulk modulus, were determined through uniaxial compressive strength experiments, as shown in Table A1 in Appendix A. Higher uniaxial compressive strength increases material resistance to compression. A greater elastic modulus indicates increased resistance to deformation. Poisson's ratio reflects material volume change; higher ratios suggest susceptibility to lateral expansion under pressure. A higher

shear modulus indicates a lower resistance to shear deformation. Conversely, a higher bulk modulus indicates greater resistance to volume changes.

5.1. Compressive Strength

The uniaxial compressive strength is a crucial mechanical property of rocks. Rock damage occurs when the pressure applied exceeds the compressive strength of the rock. Consequently, the compressive strength of the rock exerts a direct influence on its capacity to successfully press open and break up the formation during the hydraulic fracturing process. The compressive strength of the rock has a direct impact on the efficacy of fracturing. In general, the higher the compressive strength, the more challenging it is to form a fracture network following rock fracturing [22,23].

In order to ascertain the compressive strength of each rock sample, uniaxial compressive strength experiments were conducted, the results of which are presented in Table A1 in Appendix A.

It is possible to accurately assess the compressive strength of rock through indoor core experiments. However, there is a lack of continuity in the methods used for indoor evaluation. Compressive strength continuum profiles can be derived from logging data. Miller and Deere established a statistical relationship between the uniaxial compressive strength, elastic modulus, and mud content of rock, as depicted in Equation (1), following experiments on over 200 rocks [24]. The volumetric mud content is estimated using natural gamma logging data, employing the relative value method, as detailed in Equations (2) and (3).

$$\sigma_c = 0.0045E_d(1 - V_{cl}) + 0.008V_{cl}E_d \tag{1}$$

$$V_{cl} = \frac{2^{GCUR \cdot I_{GR}} - 1}{2^{GCUR} - 1} \tag{2}$$

$$I_{GR} = \frac{GR - GR_{\min}}{GR_{\max} - GR_{\min}} \tag{3}$$

In the aforementioned formula, σ_c represents the compressive strength in megapascals; E_d represents the static elastic modulus in megapascals; V_{cl} stands for the mud content, dimensionless; I_{GR} denotes the mud content index, dimensionless; and GR, GR_{max}, GR_{min} corresponds to the natural gamma values in API for the destination layer, pure mudstone layer, and pure sandstone layer, respectively. The maximum value of 134.92 and the minimum value of 35.213 were derived from the GR logging data. GCUR represents Hirch's index, which is assigned a value of 3.7 for tertiary formations and 2 for older formations. In this paper, drilling encounters occur in the tertiary and quaternary systems; thus, the value of 3.7 is utilized.

If the rock is assumed to behave as an isotropic infinite elastomer, the dynamic elastic modulus and dynamic Poisson's ratio are calculated using longitudinal and transverse wave velocities, as detailed in Equations (4) and (5) [24].

$$E_{\mathrm{d}} = \frac{\rho V_S^2(3V_p^2 - 4V_s^2)}{(V_p^2 - 2V_s^2)} \tag{4}$$

$$\mu_d = \frac{(V_p^2 - 2V_s^2)}{2(V_p^2 - V_s^2)} \tag{5}$$

where E_d represents the static elastic modulus in MPa; μ_d stands for the dynamic Poisson's ratio; V_p denotes the longitudinal wave velocity in m/s; V_s signifies the transverse wave velocity in m/s; and ρ indicates the bulk density of the rock in g/cm^3.

The compressive strength calculated by Equation (1) exhibits a lower error rate compared to the indoor core experiments. Consequently, the formula can be utilized to ascertain the compressive strength of the entire well section.

5.2. Brittleness Index

The brittleness index is a measure of the ease with which a rock may fracture. Furthermore, it reflects the ease with which cracks propagate and complex fracture networks are formed following fracturing [25–27]. It is widely acknowledged that in the fracking process, more sensitive formations require special attention. The stratigraphic properties of this formation are characterized by hardness and brittleness, which result in a high brittleness index. This type of formation can undergo fracturing to rapidly form a complex network of seams [23,28–30]. However, in instances where the formation is resistant to fracturing or where the formation it is challenging or the formation to fracture in order to form a complex network of seams, the brittleness index is typically low.

Minerals such as quartz, feldspar, and carbonate rocks are typically regarded as brittle minerals. The greater the proportion of these minerals, the greater the brittleness of the rock. Equation (6) provides the relationship between the rock brittleness index and mineral composition.

$$B_{rit1} = \frac{W_{qtz} + W_{carb}}{W_{total}} \tag{6}$$

In the equation, B_{rit1} represents the rock brittleness index obtained using the mineral composition method; W_{qtz} represents the content of quartz and feldspar; W_{carb} represents the content of carbonate rocks; and W_{total} represents the quantity of all minerals in the rock.

X-ray diffraction mineralogical analysis (XDMA) is a widely utilized experimental method for the analysis of the composition and content of rock minerals. The X-ray diffraction distribution curve of the specimen is illustrated in Figure 9. The mineral fraction is predominantly composed of clastic sandstone and quartz sandstone. The quartz content ranged from 33.0% to 90%, with an average of 63.75%. The principal types of rock debris include kyanite (10.53%), eruptive rocks (2.89%), and mica (2.75%). The principal fillers include hydromica (2.51%), siliceous (2.32%), chlorite (1.98%), and kaolinite (1.43%).

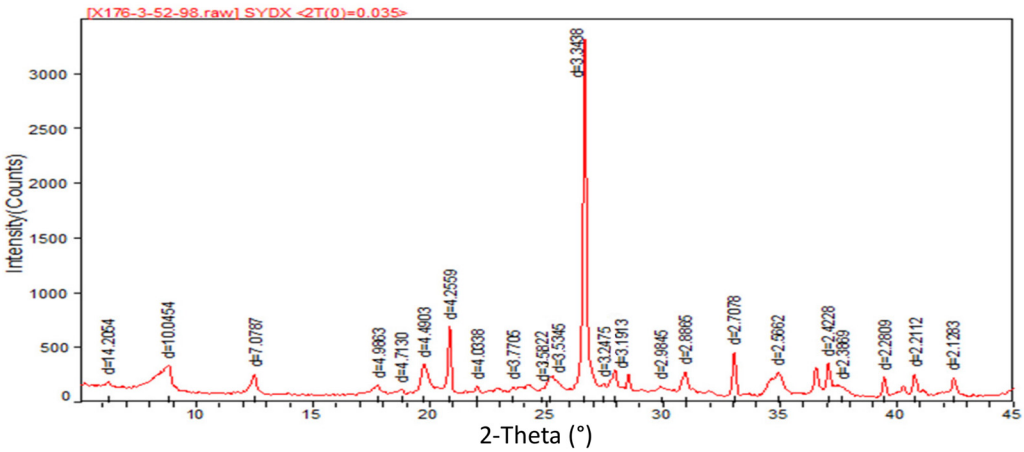

Figure 9. X-ray energy spectrum of rock.

Following a theoretical analysis of the formation mechanism of rock brittleness, Rickman proposed a parametric approach within elastic mechanics. The evaluation of reservoir brittleness using the elastic modulus and Poisson's ratio was conducted [31]. The elastic modulus and Poisson's ratio, as determined from uniaxial compressive strength experiments, are presented in in Table A1 in Appendix A. A larger Poisson's ratio is indicative of a smaller elastic modulus, which is indicative of a lower brittleness of the rock [32]. This method is a widely utilized and reliable approach for evaluating the brittleness of rocks. The calculation formula is depicted in Equation (7):

$$B_{rit2} = 0.5E_{Brit} + 0.5\mu_{Brit} = 0.5\frac{E - E_{\min}}{E_{\max} - E_{\min}} + 0.5\frac{\mu_{\max} - \mu}{\mu_{\max} - \mu_{\min}} \tag{7}$$

In the equation, B_{rit2} is the standardized brittleness index, dimensionless; E_{Brit} and μ_{Brit} are the standardized elastic modulus and Poisson's ratio, respectively, dimensionless; E, E_{max} and E_{min} are the static elastic modulus, maximum, and minimum elastic modulus within the region, in units of MPa; and μ, μ_{max}, and μ_{min} are the static Poisson's ratio, maximum, and minimum Poisson's ratio within the region, dimensionless.

After the linear regression analysis of the elastic parameters derived from dynamic and static simultaneous tests [24], utilizing logging data and in-house core experiments, the objective is to obtain the elastic modulus and Poisson's ratio of the rock in the static state, as well as their conversion relationship with the elastic modulus and Poisson's ratio in the dynamic state. Equations (8) and (9) provide a description of this phenomenon:

$$E = 0.6042E_d - 0.1989 \tag{8}$$

$$\mu = 0.18 + 0.3\mu_d \tag{9}$$

where E_d represents the static elastic modulus in MPa; μ_d represents the dynamic Poisson's ratio; E represents the static elastic modulus in MPa; and μ represents the static Poisson's ratio.

The objective of this study was to analyze the mineral composition, reservoir elastic modulus, and Poisson's ratio of oil and gas reservoirs in the Yihuang New Area by integrating mineral composition analysis with elastomechanical parametric methods. A brittleness index formula was developed to accommodate the specific characteristics of the new Yihuang district within the study area. The equation is presented in Equation (10), and the results of the brittleness index are displayed in Table 1.

$$B_{rit} = B_{rit1} \times B_{rit2} \tag{10}$$

Table 1. Brittleness index results.

Well Number	Well Depth (m)	Stratigraphic Unit	Brittleness Index 1	Brittleness Index 2	Brittleness Index
Yi 70 Well	1320–1323 m	Shan 1	0.78	0.79	0.61
Yi 70 Well	1350–1355 m	Shan 1	1.67	0.49	0.82
Yi 70 Well	1355–1360 m	Shan 1	0.87	0.28	0.24
Yi 10-1-26 Well	2487–2495 m	Shanxi	0.67	0.94	0.63
Yi 10-1-26 Well	2503–2512 m	Shanxi	0.63	0.27	0.17
Yi 10-1-26 Well	2585–2587 m	Taiyuan	0.98	0.27	0.27
Yi 10-1-26 Well	2589–2591 m	Taiyuan	0.97	0.35	0.34
Yi 76 Well	1870–1875 m	Box 8	0.06	0.50	0.03
Yi 76 Well	1921–1925 m	Shan 1	0.76	0.31	0.24
Yi 76 Well	1925–1930 m	Shan 1	0.78	0.50	0.39

5.3. Bulk Modulus

Bulk modulus is a physical property that describes the extent to which a rock or other material undergoes volumetric change when subjected to uniform external pressure. The bulk modulus is calculated from parameters such as the elastic modulus and Poisson's ratio of the rock, utilizing elasticity theory. It is common practice to derive an expression for the bulk modulus from the elastic modulus and Poisson's ratio of a rock.

The elastic modulus and Poisson's ratio can be determined from indoor core experiments. Equation (11) elucidates the interrelationship between the bulk modulus (K), elastic modulus (E), and Poisson's ratio (ν):

$$K = \frac{E}{3(1-2\nu)} \tag{11}$$

where E represents the elastic modulus of the material, and v represents the Poisson's ratio.

The bulk modulus is obtained from Equation (11) and is presented in Table A1 in Appendix A.

However, the bulk modulus data obtained by the aforementioned equation are discrete and discontinuous. It is possible to derive continuous profiles of the bulk modulus from logging data. The bulk modulus of rock is typically correlated with the density of the rock, as well as the transverse- and longitudinal-wave velocities [24]. The generalized expression is depicted in Equation (12).

$$K_b = \rho(V_p^2 - \frac{4}{3}V_s^2) \times 10^{-3} \tag{12}$$

where ρ is the bulk density of the rock in g/cm³; and Vs and Vp are the transverse and longitudinal wave velocities of the rock in m/s.

In the majority of oilfield logging operations, full wave-train logging is not employed. The data pertaining to transverse waves are absent. Consequently, the transverse-wave velocity is estimated using empirical equations that are specific to the given stratum. For the majority of strata, a commonly utilized regression-based empirical formula is depicted in Equation (13) [24]. Acoustic velocity logging is a method of measuring the time difference (ΔT), the longitudinal time difference (Δt_p), and the transverse time difference (Δt_s) of a glide wave propagating through a formation. The longitudinal-wave velocity Vp is obtained through conversion, as shown in Equation (14) [24].

$$V_s = \sqrt{11.44V_p + 18.03} - 5.686 \tag{13}$$

$$V_p = \frac{1}{\Delta t_p} \tag{14}$$

where Vs and Vp represent the transverse- and longitudinal- wave velocities of the rock in m/s; and Δtp denotes the longitudinal-wave time difference.

The bulk modulus calculated using the aforementioned equation exhibits a lower degree of error compared to that observed in indoor testing. Consequently, the bulk modulus for the entire well section can be determined.

Previous studies have demonstrated a correlation between higher bulk-modulus values and greater difficulty in fracturing the rock. This suggests that the formation of a fracture network following rock fracturing is challenging [33].

5.4. Shear Modulus

The shear modulus is defined as the ability of a material to resist deformation under a shear force. It is frequently employed to describe the stiffness of a material. It is a crucial parameter in the characterization of rock mechanical properties. A common approach involves the use of the rock's elastic modulus and Poisson's ratio to derive the bulk-modulus expression.

The elastic modulus and Poisson's ratio can be determined through indoor core experiments. The relationship between shear modulus (G) and elastic modulus (E) and Poisson's ratio (ν) is depicted in Equation (15).

$$G = \frac{E}{2(1+\nu)} \tag{15}$$

where E represents the elastic modulus of the material, and ν represents Poisson's ratio.

The shear modulus is calculated using Equation (15) and is presented in Table A1 in Appendix A. However, the shear modulus data obtained from the aforementioned equation are discrete and discontinuous. It is possible to derive continuous profiles of the shear modulus from logging data. The shear modulus of rock is typically associated with the density and transverse-wave velocity of the rock [24]. Its general expression is depicted in Equation (16).

$$G_b = \rho V_s^2 \times 10^{-3} \tag{16}$$

where ρ represents the bulk density of the rock in g/cm³, and Vs denotes the transverse-wave velocity of the rock in m/s.

The shear modulus calculated using the above equation exhibits less error compared to indoor testing. Therefore, the shear modulus for the entire well section can be determined.

Studies have shown that higher shear-modulus values correspond to easier rock fracturing. It is also easier to form a fracture network after stone fracturing [34].

5.5. Horizontal-Stress Differential Coefficient

It is a well-established fact that geostress is a natural phenomenon that occurs in rock formations. It is intimately connected to the formation of fractures during the fracking process. To some extent, it controls the direction and extent of fractures formed during fracturing [35]. When the horizontal-stress difference coefficient is minimal, fractures formed during the fracturing process can extend in multiple directions, which is a crucial factor in the formation of complex fracture networks [36]. When the horizontal-stress differential coefficient is considerable, cracks exhibit greater singularity in terms of their extension range and pattern. The primary mode of expansion is in the direction of the maximum horizontal principal stress.

Positive stresses at Kessel points in three horizontally oriented cores, spaced 45° apart, were measured using mechanical experiments. Substitution of these values into Equations (17)–(19) yields the following results: the obtained results represent the maximum and minimum principal geopathic stresses applied to the specimen downhole.

$$\sigma_H = \frac{\sigma_1 + \sigma_3}{2} + \frac{\sigma_1 - \sigma_3}{2}\sqrt{1 + \tan^2 2\alpha} + \alpha p_p - p_c \tag{17}$$

$$\sigma_h = \frac{\sigma_1 + \sigma_3}{2} - \frac{\sigma_1 - \sigma_3}{2}\sqrt{1 + \tan^2 2\alpha} + \alpha p_p - p_c \tag{18}$$

$$\tan 2\alpha = \frac{\sigma_1 + \sigma_3 - 2\sigma_2}{\sigma_1 - \sigma_3} \tag{19}$$

where σ_1, σ_2, and σ_3 represent the Kessel-point positive stresses in three cores spaced 45° apart horizontally.

σ_H, σ_h represent the maximum and minimum principal stresses.

α represents the effective stress contribution factor.

p_p represents the formation pore pressure.

p_c represents the confining pressure to which the core is subjected in the high-pressure wellbore.

The maximum and minimum principal stresses are derived from the above equation.

The magnitude of the horizontal principal-stress difference is typically quantified by the horizontal-stress differential coefficient. The formula is shown in Equation (20).

$$K_h = \frac{\sigma_H - \sigma_h}{\sigma_h} \tag{20}$$

where K_h represents the horizontal-stress difference coefficient; σ_H denotes the maximum horizontal principal stress in MPa; and σ_h indicates the minimum horizontal principal stress in MPa.

The maximum and minimum ground stresses, as well as the horizontal- stress difference coefficient, are obtained from the above equation, and the results are presented in Table 2.

Studies have demonstrated that rocks are more susceptible to fracturing when the horizontal-stress difference coefficient is below 0.3. The greater the amount by which the horizontal-stress difference coefficient exceeds 0.5, the more challenging it becomes to form a fracture network after rock fracturing [36].

Table 2. Calculation results of horizontal stress.

Well Number	Well Depth (m)	Stratum	Maximum Earth Stress	Minimum Earth Stress	Horizontal Stress Differential Coefficient
Yi 70 Well	1320–1323 m	Shan 1	17.21	10.19	0.69
Yi 70 Well	1350–1355 m	Shan 1	18.91	10.99	0.72
Yi 70 Well	1355–1360 m	Shan 1	41.88	26.12	0.60
Yi 10-1-26 Well	2487–2495 m	Shanxi	22.43	15.67	0.43
Yi 10-1-26 Well	2503–2512 m	Shanxi	39.41	17.09	1.31
Yi 10-1-26 Well	2585–2587 m	Taiyuan	33.56	17.24	0.95
Yi 10-1-26 Well	2589–2591 m	Taiyuan	25.53	18.25	0.39
Yi 76 Well	1870–1875 m	Box 8	34.65	24.35	0.42
Yi 76 Well	1921–1925 m	Shan 1	41.21	26.79	0.54
Yi 76 Well	1925–1930 m	Shan 1	82.13	64.87	0.27

5.6. Fracture Toughness

Fracture toughness is employed primarily to assess the ease of reservoir fracturing. Additionally, it indicates whether the crack can propagate forward. The lower the fracture toughness of the reservoir, the easier it is for the fractures created during hydrophilic fracturing to propagate forward. The more the rock can undergo deformation, and in addition, the lower the fracture toughness, the easier it is to conduct fracturing. The structure of the fracture network formed after fracturing becomes increasingly complex, which is conducive to achieving improved fracturing outcomes [37]. To enhance the fracturing volume in the Yihuang New Area reservoirs, it is necessary for hydrostatic fractures to connect to natural fractures.

To examine the fracture toughness of oil and gas reservoirs in the Yihuang New Area, the fracture-toughness prediction models of types I and II, established by Chen et al., using logging data, are employed in this paper [38]. Figure 10 depicts the mud content and acoustic time-difference curves for a number of wells. The fracture-toughness results obtained from Equations (21) and (22) are presented in Table 3.

$$K_{IC} = 0.450\rho - 0.151\exp(V_{cl}) + 0.201\ln(AC) - 0.877 \quad (21)$$

$$K_{IIC} = 2.119\rho - 0.245\exp(V_{cl}) + 1.152\ln(AC) - 0.8378 \quad (22)$$

where K_{IC} represents Type I fracture toughness, measured in MPa. $m^{0.5}$; K_{IIC} represents Type II fracture toughness; ρ is the sandstone density, measured in g/cm^3; V_{sh} is the clay content, measured in %; and AC is the sonic time difference, measured in μs/ft.

Table 3. Fracture-toughness parameters of research section in Yihuang New Area.

Well Number	Well Depth (m)	The Clay Content	Fracture Toughness
Yi 70 Well	1350–1355 m	0.173	0.9941
Yi 70 Well	1320–1323 m	0.173	0.9941
Yi 70 Well	1355–1360 m	0.173	0.9941
Yi 76 Well	1870–1875 m	0.143	0.9972
Yi 76 Well	1925–1930 m	0.114	0.9935
Yi 76 Well	1921–1925 m	0.175	0.993
Yi 10-1-26 Well	2487–2495 m	0.2412	0.993
Yi 10-1-26 Well	2585–2587 m	0.102	0.833
Yi 10-1-26 Well	2589–2591 m	0.097	0.934
Yi 10-1-26 Well	2503–2512 m	0.243	0.993

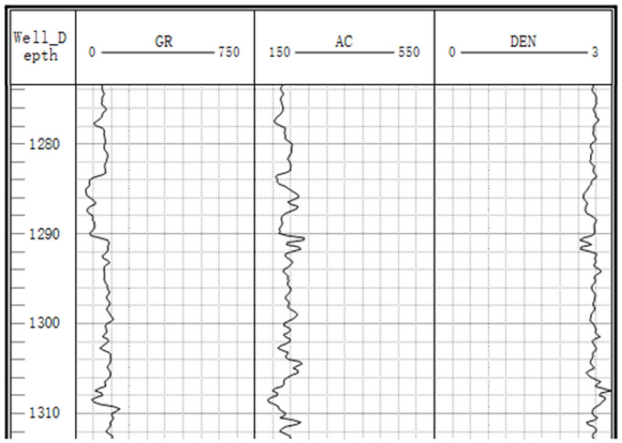

(a) Yi 70 Well

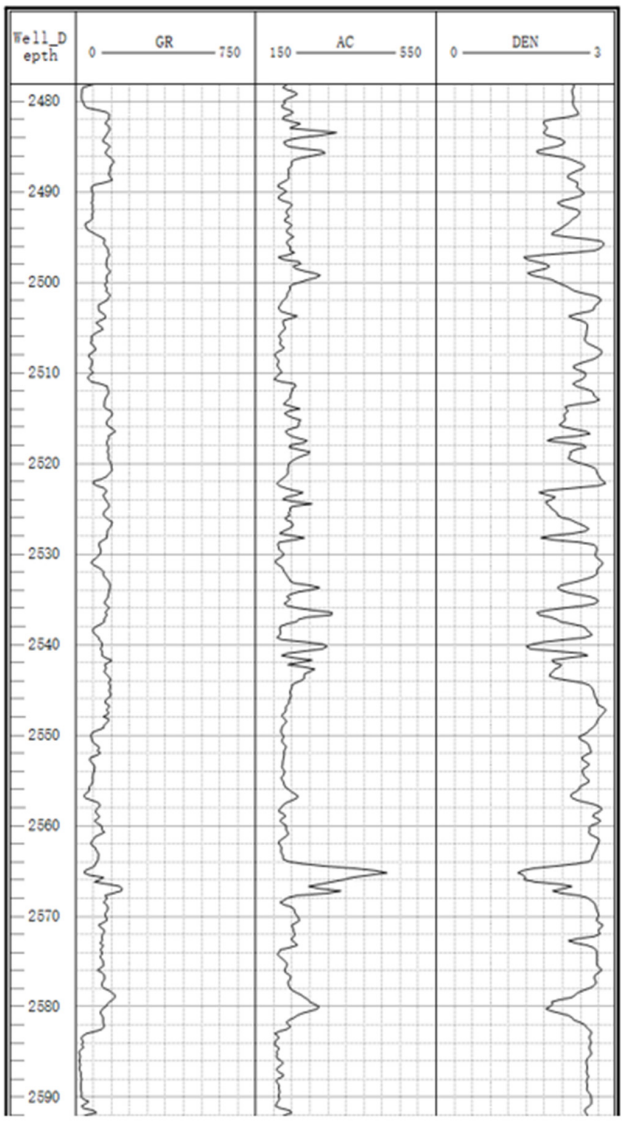

(b) Yi 10-1-26 well

Figure 10. *Cont*.

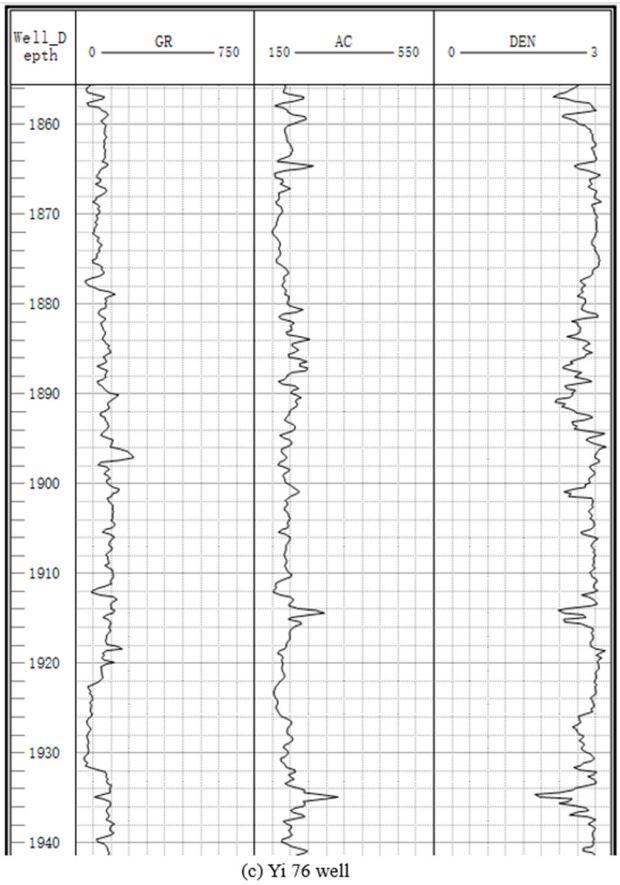

Figure 10. Mud content and acoustic time-difference curves for different wells.

6. Catastrophe Theory

6.1. Basic Principles

The field of catastrophe theory was first proposed by the French mathematician René Thom [39]. The primary application of catastrophe theory is the study of the effects of continuous variations in independent variables (inputs) [40] on abrupt changes in behavior (outputs). A dynamical system M can be represented by a smoothing function f incorporating multi-dimensional input variables (control variables and parameters) and multidimensional output variables (response variables and behavior). Previous studies have demonstrated the particular relevance of catastrophe theory for the analysis of uncertain systems, with extensive applications across a range of disciplines [41].

From the perspective of catastrophe theory, the critical points of the potential energy function V(x) constitute an equilibrium surface. Here, x represents the system's behavioral state as a state variable, while u, v, w, and t denote control variables [41–44]. The equation of this plane is derived by computing the first-order derivative $V'(x) = 0$ of V(x). The set of singularities is determined by computing the second-order derivative $V''(x) = 0$ of V(x). By eliminating x from the equations $V'(x) = 0$ and $V''(x) = 0$, the equations defining the divergent point set for the catastrophe system can be derived. Four common models exist in catastrophe theory: fold catastrophe, cusp catastrophe, swallowtail catastrophe, and butterfly catastrophe. These are described in detail in [45–48]. Table 4 presents the potential functions and equations defining the divergent point sets for the four common models.

Table 4. Four common catastrophe models.

Category	Potential Function	Bifurcation Set
Fold catastrophe	$V(x) = x^3 + ux$	$u = 0$
Cusp catastrophe	$V(x) = x^4 + ux^2 + vx$	$u = -6x^2$, $v = 8x^3$
Swallowtail catastrophe	$V(x) = x^5 + ux^3 + vx^2 + wx$	$u = -6x^2$, $v = 8x^3$, $w = -3x^4$
Butterfly catastrophe	$V(x) = x^6 + ux^4 + vx^3 + wx^2 + tx$	$u = -10x^2$, $v = 20x^3$, $w = -15x^4$, $t = 4x^5$

6.2. Normalized Formula for Catastrophe Models

The normalization formula can be derived from the decomposition form of the divergence point-set equation for the catastrophe system. Consequently, the total catastrophe-affiliation function value for the system can be determined. The normalization formulas for the four common catastrophe models are provided in Equations (23)–(26) [43–46].

$$\text{Fold catastrophe}: \ x_u = \sqrt{u} \tag{23}$$

$$\text{Cusp catastrophe}: \ x_u = \sqrt{u}, \ x_v = \sqrt[3]{v} \tag{24}$$

$$\text{Swallowtail catastrophe}: \ x_u = \sqrt{u}, \ x_v = \sqrt[3]{v}, \ x_w = \sqrt[4]{w} \tag{25}$$

$$\text{Butterfly catastrophe}: \ x_u = \sqrt{u}, \ x_v = \sqrt[3]{v}, \ x_w = \sqrt[4]{w}, \ x_t = \sqrt[5]{t} \tag{26}$$

6.3. Evaluation Principles and Methods

In practice, three principles are used to judge the normalization formulas for comprehensive assessment [49]: the non-complementarity principle, the complementarity principle, and the post-threshold complementarity principle.

The x-values calculated for various evaluation indicators of the same object using normalization formulas are treated differently based on specific circumstances, in accordance with the three principles previously mentioned: the non-complementary principle, the complementary principle, and the complementary principle after exceeding the threshold value. In the event that the control variables of the system are unable to be substituted for one another, that is, they are unable to compensate for one another's deficiencies, then the values are taken according to the "take the middle of the largest and the smallest" standard. This is the only way in which the divergence equation can be satisfied and qualitative changes can occur. When there are no prerequisites for the indicators of the system to complement each other's deficiencies and achieve a higher average value of x, the complementarity principle is satisfied, and values are taken based on the "average value". In the case of a system that necessitates the fulfillment of certain threshold conditions before the indicators can complement each other's deficiencies in order to achieve a higher average value of x, the principle of complementary after threshold is satisfied, and values are taken based on the "average value after meeting the threshold" standard [50].

7. Establishment and Application of a Comprehensive Evaluative Model for Hydraulic Fracturing Tendency

7.1. Establishment of the Evaluation Model

7.1.1. Catastrophe Model

The hydraulic fracturing tendency of sandstone reservoirs is largely determined by the interaction of numerous influencing factors. This paper posits that positive and negative correlates operate independently of each other. However, within the system, these factors interact with and constrain each other. Consequently, these factors exert a significant influence on the hydraulic fracturing tendency of sandstone reservoirs.

The brittleness index, shear modulus, compressive strength, horizontal-stress variance factor, fracture toughness, and bulk modulus were selected based on the mechanical properties of the region. These factors significantly influence the hydraulic fracturing tendency of sandstone reservoirs. Therefore, a multilevel model for sandstone reservoir

hydraulic fracturing-tendency evaluation was established, as shown in Figure 11, with the following composition:

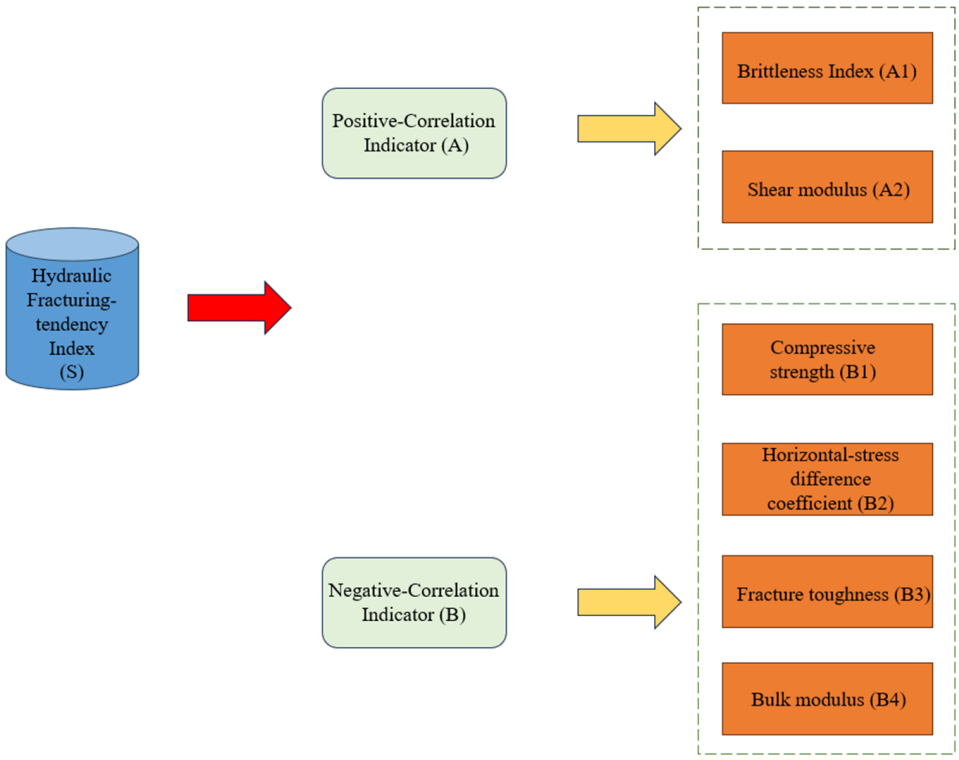

Figure 11. Hierarchical structure of influencing factors of sandstone reservoir hydraulic- fracturing tendency.

The sandstone reservoir hydraulic fracturing-tendency assessment (S) is taken as the target layer. The positive correlation indicator (A) and negative correlation indicator (B) are used as the criterion layer. The brittleness index (A1) and shear modulus (A2) are used as indicator layers for positive-correlation indicators. Compressive strength (B1), horizontal-stress differential coefficient (B2), fracture toughness (B3), and bulk modulus (B4) were employed as indicator layers for negative-correlation indicators. Based on the fundamentals of catastrophe theory [43–46], subsystems are classified based on the number of indicators included in their catastrophe models. Two categories of cusp catastrophes were recognized, and the following categories were identified: (S, A, and B) and (A, A1, and A2). One group of butterfly catastrophes was identified: (B, B1, B2, B3, and B4).

7.1.2. Dimensionalization of Control Variables

In this paper, the positive indicators are the brittleness index and shear modulus. Consequently, an increase in the index correlates with enhanced effectiveness of reservoir fracturing. Negative indicators include compressive strength, horizontal-stress differential coefficient, fracture toughness, and bulk modulus. Consequently, as the index increases, reservoir fracturing becomes less effective. The positive and negative indicators are calculated in accordance with Equations (27) and (28).

$$\text{Positive} - \text{indicator calculation formula}: \ Y = \frac{X - X_{\min}}{X_{\max} - X_{\min}} \tag{27}$$

$$\text{Negative} - \text{indicator calculation formula}: \ Y = \frac{X_{\max} - X}{X_{\max} - X_{\min}} \tag{28}$$

In the formula, Y represents the standardized parameter value; X_{max} and X_{min} represent the maximum and minimum values of the parameters in the study area, respectively; and X represents the parameter value of the target layer section.

The sandstone-reservoir hydraulic fracturing-tendency evaluation indexes were dimensionless using Equations (27) and (28), and the results are presented in Table 5.

Table 5. Standardized results of evaluation indicators for different wells.

Well Number	Well Depth (m)	Compressive Strength	Bulk Modulus	Shear Modulus	Brittleness Index	Horizontal-Stress Difference Coefficient	Fracture Toughness
Yi 70 Well	1320–1323 m	0.24	0.29	0.59	0.73	0.60	0.02
Yi 70 Well	1350–1355 m	0.27	0.85	0.52	1	0.57	0.02
Yi 70 Well	1355–1360 m	0.91	0.76	0.17	0.27	0.68	0.02
Yi 10-1-26 Well	2487–2495 m	0.17	0.23	0.90	0.76	0.85	0.03
Yi 10-1-26 Well	2503–2512 m	0.08	0.54	0.38	0.18	0	0.03
Yi 10-1-26 Well	2585–2587 m	0.34	0.86	0.24	0.30	0.35	1
Yi 10-1-26 Well	2589–2591 m	0.96	0.62	0.22	0.39	0.88	0.38
Yi 76 Well	1870–1875 m	0.08	0.83	0.28	0	0.86	0
Yi 76 Well	1921–1925 m	0.50	0.87	0.30	0.27	0.74	0.03
Yi 76 Well	1925–1930 m	0.68	0.99	0.17	0.46	1	0.02

7.1.3. Parameter Normalization

The application of multi-criteria evaluation methods is carried out in accordance with catastrophe theory. The normalization formula for catastrophe systems is employed. The catastrophe affiliation function should be calculated layer by layer, with consideration given to the indicator, criterion, and target layers. The specific calculation process is as follows:

Figures 5 and 11 illustrate the cusp catastrophe involving indicator layers A1 and A2. To illustrate, the calculation is conducted according to Equation (24) using the Yi 70 well with depths ranging from 1320 m to 1323 m, as an example.

$$X_{A1} = \sqrt{A1} = \sqrt{0.73} = 0.854,\ X_{A2} = \sqrt[3]{A2} = \sqrt[3]{0.59} = 0.839$$

The principle of complementarity is satisfied through interactions between indicator layers and their role in relation to the guideline layer. The mean value is calculated, resulting in

$$A = \frac{X_{A1} + X_{A2}}{2} = \frac{0.854 + 0.839}{2} = 0.847$$

The indicator layers B1, B2, B3, and B4 collectively represent a butterfly catastrophe. To illustrate, the calculation is conducted according to Equation (26) using the Yi 70 well with depths ranging from 1320 m to 1323 m, as an example.

$$X_{B1} = \sqrt{B1} = \sqrt{0.24} = 0.490,\ X_{B2} = \sqrt[3]{B2} = \sqrt[3]{0.60} = 0.843$$

$$X_{B3} = \sqrt[4]{B3} = \sqrt[4]{0.02} = 0.376,\ X_{B4} = \sqrt[5]{B4} = \sqrt[5]{0.29} = 0.781$$

The interactions within the indicator layer jointly influence the criterion layer, with the average value being taken according to the principle of complementarity.

$$B = \frac{X_{B1} + X_{B2} + X_{B3} + X_{B4}}{4} = \frac{0.490 + 0.843 + 0.376 + 0.781}{4} = 0.623$$

The criterion layers A and B also exhibit a cusp catastrophe. To illustrate, the calculation is conducted according to Equation (24) using the Yi 70 well with depths ranging from 1320 m to 1323 m, as an example.

$$X_A = \sqrt{A} = \sqrt{0.847} = 0.920,\ X_B = \sqrt[3]{B} = \sqrt[3]{0.623} = 0.854$$

The same principle as above applies, with the average value being taken.

$$S = \frac{X_A + X_B}{2} = \frac{0.920 + 0.854}{2} = 0.887$$

Similarly, the hydraulic fracturing-tendency evaluation values of the sandstone reservoirs of other wells can be obtained in accordance with the detailed instructions provided in Table 6.

Table 6. Catastrophe evaluation results of sandstone reservoir hydraulic-fracturing tendency.

Well Number	Well Depth (m)	Stratum	A1	A2	A	B1	B2	B3	B4	B	S
Yi 70 Well	1320–1323 m	Shan 1	0.854	0.839	0.847	0.490	0.843	0.376	0.781	0.623	0.887
Yi 70 Well	1350–1355 m	Shan 1	1	0.804	0.902	0.520	0.829	0.376	0.968	0.673	0.913
Yi 70 Well	1355–1360 m	Shan 1	0.520	0.554	0.537	0.954	0.879	0.376	0.947	0.789	0.829
Yi 10-1-26 Well	2487–2495 m	Shanxi	0.874	0.965	0.919	0.412	0.947	0.416	0.745	0.630	0.908
Yi 10-1-26 Well	2503–2512 m	Shanxi	0.424	0.724	0.574	0.283	0	0.416	0.884	0.396	0.746
Yi 10-1-26 Well	2585–2587 m	Taiyuan	0.548	0.621	0.585	0.583	0.705	1	0.970	0.815	0.850
Yi 10-1-26 Well	2589–2591 m	Taiyuan	0.624	0.604	0.614	0.980	0.958	0.785	0.909	0.908	0.876
Yi 76 Well	1870–1875 m	Box 8	0	0.654	0.327	0.283	0.951	0	0.963	0.549	0.696
Yi 76 Well	1921–1925 m	Shan 1	0.520	0.669	0.595	0.707	0.905	0.416	0.973	0.750	0.841
Yi 76 Well	1925–1930 m	Shan 1	0.678	0.554	0.616	0.825	1	0.376	0.998	0.780	0.853

As illustrated in Figure 12, the higher the hydraulic fracturing-tendency evaluation values, the easier it is to perform fracturing. The structure of the fracture network that is formed subsequent to fracturing becomes increasingly complex. Furthermore, the effectiveness of fracking is enhanced. The hydraulic fracturing-tendency evaluation values for well Yi 70 are 0.829, 0.913, and 0.887; for well Yi 10-1-26, they are 0.876, 0.850, 0.746, and 0.908; and for well Yi 76, they are 0.853, 0.841, and 0.696. In light of the aforementioned considerations, a comprehensive analysis of the hydraulic fracturing-tendency evaluation values for the Yi70, Yi10-1-26, and Yi 76 wells is warranted. The hydraulic fracturing tendency of sandstone reservoirs in the study area is classified into three categories. Reservoirs with hydraulic fracturing-tendency evaluation values greater than 0.8 are classified as Class I reservoirs, which are defined as having good hydraulic-fracturing tendency. Reservoirs with hydraulic fracturing-tendency evaluation values between 0.7 and 0.8 are classified as Class II reservoirs with average hydraulic-fracturing tendency. Reservoirs with hydraulic fracturing-tendency evaluation values less than 0.7 are classified as Class III reservoirs with poor hydraulic-fracturing tendency. The results of the preferred fracturing stratigraphy for wells Yi70, Yi10-1-26, and Yi76 in the study area should be finalized. Among the wells, the Yi 70 well at depths of 1320–1323 m, 1350–1355 m, and 1355–1360 m exhibited the most favorable hydraulic-fracturing tendency. These layers may be selected for fracture modification in the Yi 70 well. The sections of the Yi 10-1-26 well at depths of 2487–2495 m, 2585–2587 m and 2589–2591 m exhibit good hydraulic-fracturing tendency. This layer may be a preferred candidate for fracture modification in the Yi 10-1-26 well. The Yi 76 well at depths of 1921–1925 m and 1925–1930 m exhibits pressurized conditions. This layer may be considered the optimal zone for fracture modification in the Yi 76 well.

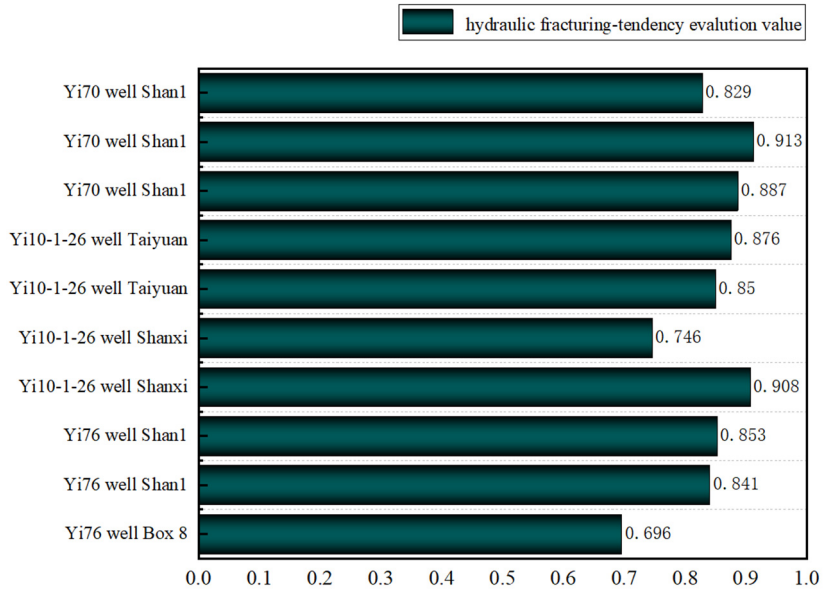

Figure 12. Hydraulic fracturing-tendency catastrophe evaluation results of different wells in Yihuang New Area.

7.2. Analytic Hierarchy Process (AHP)

To validate the practicality of applying catastrophe theory to evaluate hydraulic fracturing tendency in sandstone reservoirs, the Analytic Hierarchy Process was employed to compute the hydraulic fracturing-tendency index for each of the aforementioned wells.

The hierarchy of influencing factors and the judgment matrix were established in accordance with the Analytic Hierarchy Process. The eigenvector of this matrix, denoted as A = (0.31, 0.17, 0.09, 0.09, 0.17, 0.17), must be obtained. Consequently, the final hydraulic fracturing-tendency index (FI) is derived as depicted in Equation (29).

$$FI = 0.31B_{rit} + 0.17\sigma_c + 0.09K + 0.09G + 0.17K_h + 0.17K_c \quad (29)$$

In the formula, FI represents the hydraulic fracturing-tendency index; B_{rit} stands for the dimensionless brittleness index; σ_c denotes the dimensionless compressive-strength index; K represents the dimensionless bulk modulus; G represents the dimensionless elastic modulus; K_h stands for the dimensionless horizontal-stress difference coefficient; and K_c represents the dimensionless fracture toughness.

The hydraulic fracturing-tendency index for other wells can be calculated using the formula provided in Equation (18). The specific outcomes are presented in Table 7.

Table 7. Hydraulic fracturing tendency evaluation table determined by analytic hierarchy process.

Well Number	Well Depth (m)	Stratum	Compressive Strength	Bulk Modulus	Shear Modulus	Brittleness Index	Horizontal-Stress Difference Coefficient	Fracture Toughness	Hydraulic Fracturing-Tendency Index
Yi 70 Well	1320–1323 m	Shan 1	0.24	0.29	0.59	0.73	0.60	0.02	0.45
Yi 70 Well	1350–1355 m	Shan 1	0.27	0.85	0.52	1	0.57	0.02	0.58
Yi 70 Well	1355–1360 m	Shan 1	0.91	0.76	0.17	0.27	0.68	0.02	0.44
Yi 10-1-26 Well	2487–2495 m	Shanxi	0.17	0.23	0.90	0.76	0.85	0.03	0.52
Yi 10-1-26 Well	2503–2512 m	Shanxi	0.08	0.54	0.38	0.18	0	0.03	0.16
Yi 10-1-26 Well	2585–2587 m	Taiyuan	0.34	0.86	0.24	0.30	0.35	1	0.48
Yi 10-1-26 Well	2589–2591 m	Taiyuan	0.96	0.62	0.22	0.39	0.88	0.38	0.57
Yi 76 Well	1870–1875 m	Box 8	0.08	0.83	0.28	0	0.86	0	0.26
Yi 76 Well	1921–1925 m	Shan 1	0.50	0.87	0.30	0.27	0.74	0.03	0.40
Yi 76 Well	1925–1930 m	Shan 1	0.68	0.99	0.17	0.46	1	0.02	0.54

Figure 13 illustrates the fact that a higher hydraulic fracturing-tendency index is conducive to fracturing. The fracturing process becomes more effective, resulting in the formation of a more complex fracture network post-fracturing. The optimal fracturing

strata were ultimately determined to be located at depths of 1320–1323 m, 1350–1355 m, and 1355–1360 m in the Yi70 well, as well as at depths of 2487–2495 m, 2585–2587 m and 2589–2591 m in the Yi10-1-26 well, and finally, at depths of 1921–1925 m and 1925–1930 m in the Yi76 well, within the study area.

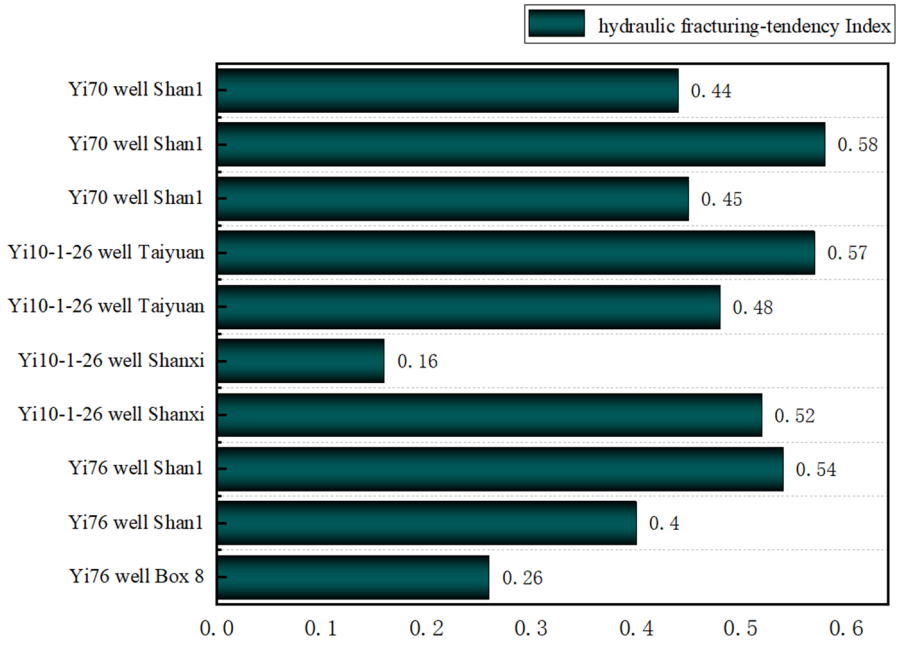

Figure 13. Hydraulic fracturing-tendency index of different wells in Yihuang New Area.

7.3. Comprehensive Evaluation

The data were calculated and analyzed from wells Yi70, Yi76, and Yi10-1-26, which are located within the study area. A comparison of Figures 12 and 13 is presented below. It can be observed that the outcomes of well sections with favorable fracturable results obtained through the application of both methodologies are largely comparable. In the study area, the Yi 70 well exhibited good hydraulic fracturing-tendency results at depths of 1320–1323 m, 1350–1355 m, and 1355–1360 m. Similarly, the Yi10-1-26 well demonstrated good hydraulic fracturing tendency at depths of 2487–2495 m, 2585–2587 m, and 2589–2591 m. Finally, the Yi76 well exhibited good hydraulic fracturing tendency at depths of 1921–1925 m and 1925–1930 m.

This study demonstrates the feasibility of applying catastrophe theory to the evaluation of sandstone reservoir hydraulic-fracturing tendency. The necessity for concurrent human assessment of weight is eliminated. The potential for subjective influence on evaluation results is eliminated, and extends eastward, predominantly.

7.4. Assessment of Post-Fracturing Effects

The sandstone reservoir hydraulic fracturing-tendency evaluation method, as outlined in the aforementioned paper, was employed in this study. A section of Shanxi Group 1, spanning 1350–1355 m, was selected for hydraulic fracturing modification in the Yi 70 well. Real-time microseismic monitoring was conducted to assess the effectiveness of the hydraulic fracturing modification. It was observed that a fracture crack oriented in a north-easterly direction was produced in this layer section. The fracturing modification is effective and achieves the purpose of fracturing and creating fracture networks. The feasibility of utilizing this method for the selective fracturing of fractured segments is demonstrated.

7.5. Directions for Future Research

In future studies, it would be beneficial to consider additional mechanical parameters when evaluating the factors influencing the hydraulic fracturing tendency of sandstone

reservoirs. Similarly, temperature and overburden pressure should be taken into account when evaluating the factors influencing the hydraulic fracturing tendency of the rock in deeper sections of the well. To ensure the accuracy of the hydraulic fracturing-tendency catastrophe evaluation results for each well, it would be advisable to cross-verify them using various compressible-fracture models.

8. Conclusions

(1) In the case of sandstone reservoirs, a comprehensive analysis of compressive strength, bulk modulus, shear modulus, brittleness index, horizontal-stress differential coefficient, and fracture toughness is conducted. In accordance with catastrophe theory, a multilevel structure is proposed for the evaluation of sandstone reservoir hydraulic-fracturing tendency, comprising a target layer, a guideline layer, and an index layer. A catastrophe model was developed for the evaluation of sandstone reservoir hydraulic-fracturing tendency. The objective of this study is to quantitatively characterize the ease with which sandstone fractures can be modified using hydraulic fracturing-tendency evaluation values. A set of hydraulic fracturing-tendency evaluation methods suitable for sandstone reservoirs has been developed.

(2) The results of the catastrophe model evaluation are in alignment with the results of the Analytic Hierarchy Process (AHP) for weight determination. This study demonstrates the efficacy of catastrophe theory in evaluating the hydraulic fracturing tendency of sandstone reservoirs. The evaluation results it provides are more accurate, in comparison to traditional methodologies. The catastrophe-theory evaluation methods are highly operational and practical. The model is not subject to the limitations of human subjectivity, and the influence of subjective interference is significantly reduced, thereby ensuring the credibility of the evaluation results.

(3) Sandstone reservoirs are classified into three categories based on the characteristics of each parameter within the reservoir and the hydraulic fracturing-tendency evaluation values. Reservoirs with hydraulic fracturing-tendency evaluation values greater than 0.8 are classified as Class I reservoirs with good hydraulic-fracturing tendency. Those with hydraulic fracturing-tendency evaluation values between 0.7 and 0.8 are classified as Class II reservoirs with average hydraulic-fracturing tendency. Finally, reservoirs with hydraulic fracturing-tendency evaluation values less than 0.7 are classified as Class III reservoirs with poor hydraulic-fracturing tendency.

(4) The hydraulic fracturing tendency of sandstone reservoirs is evaluated in accordance with established criteria. The optimal fracturing layers for the Yi70 well were identified as 1320–1323 m, 1350–1355 m, and 1355–1360 m; for the Yi10–1–26 well, 2487–2495 m, 2585–2587 m, and 2589–2591 m; and for the Yi76 well, 1921–1925 m and 1925–1930 m. The established hydraulic fracturing-tendency evaluation methodology has been demonstrated to be practical after field application.

Author Contributions: Software, Y.H.; validation, L.W.; investigation, H.H. and Y.W.; data curation, Z.Q.; writing—original draft, H.F.; writing—review and editing, P.W. All authors have read and agreed to the published version of the manuscript.

Funding: (1) In 2023: National Natural Science Foundation of China, research on prediction method using multi-scale fusion of damage and instability for wellbore rock based on machine learning (No. 52274007); (2) In 2020, National Natural Science Foundation of China, comprehensive analysis and calculation simulation of wellbore instability based on disturbance state theory, (No. 51974255); (3) In 2022, supported by the scientific research program of Shaanxi Provincial Education Department, the research on crack propagation mechanism of surrounding rock of shaft lining based on near-field dynamics, (No. 22JS028); (4) In 2022, the Science Fund for Distinguished Young Scholars, based on the CFD-EDM coupling method, studied the migration mechanism of shale oil reservoir volume fracturing proppant (No. 022JC-37).

Data Availability Statement: Data are contained within the article.

Acknowledgments: The experiments in this research program were supported by the Key Laboratory of Well Stability and Fluid and Rock Mechanics in Oil and Gas Reservoirs of Shaanxi Province. The original contributions presented in the study are included in the article; further inquiries can be directed to the corresponding author.

Conflicts of Interest: Author Yawen He was employed by the Yumen Drilling Company. The remaining authors declare that the research was conducted in the absence of any commercial or financial relationships that could be construed as a potential conflict of interest. The Yumen Drilling Company had no role in the design of the study; in the collection, analyses, or interpretation of data; in the writing of the manuscript, or in the decision to publish the results.

Appendix A

Table A1. Experimental results of compressive strength of different wells in Yichuan New Area.

Well Number	Core ID	Direction	Well Depth (m)	Stratum	Elastic Modulus (MPa)	Shear Modulus (MPa)	Poisson's Ratio	Bulk Modulus (MPa)	Compressive Strength (MPa)
Yi 70 Well	2-1/45	0	1351 m	Shan 1	2286.88	1067.594	0.071	888.538	15.47
Yi 70 Well	2-1/45	45	1351 m	Shan 1	3299.28	1644.017	0.003	1107.332	18.07
Yi 70 Well	2-1/45	90	1351 m	Shan 1	4985.05	2178.466	0.144	2334.914	19.02
Yi 70 Well	2-14/45	0	1356 m	Shan 1	7691.18	3675.286	0.05	2825.590	32.19
Yi 70 Well	2-14/45	45	1356 m	Shan 1	4196.23	2080.969	0.01	1422.182	17.48
Yi 70 Well	2-14/45	90	1356 m	Shan 1	3295.44	1745.268	−0.06	988.030	18.86
Yi 70 Well	2-39/45	0	1321 m	Shan 1	2107.21	1048.718	0.005	709.012	18.07
Yi 70 Well	2-39/45	45	1321 m	Shan 1	6189.07	3077.570	0.006	2086.020	28.51
Yi 70 Well	2-39/45	90	1321 m	Shan 1	4653.56	2237.286	0.04	1686.071	25.96
Yi 10-1-26 Well	1-72/120	0	2508 m	Shanxi	10,091.86	4831.487	0.04	3691.661	44.65
Yi 10-1-26 Well	1-72/120	45	2508 m	Shanxi	7796.57	3754.470	0.04	2814.479	42.79
Yi 10-1-26 Well	1-72/120	90	2508 m	Shanxi	6180.82	3080.779	0.003	2073.239	23.41
Yi 10-1-26 Well	1-77/120	0	2490 m	Shanxi	7712.23	3761.997	0.025	2706.145	49.44
Yi 10-1-26 Well	1-77/120	45	2490 m	Shanxi	15,093.51	7414.816	0.02	5216.820	50.70
Yi 10-1-26 Well	1-77/120	90	2490 m	Shanxi	15,196.00	7070.040	0.075	5954.665	43.44
Yi 10-1-26 Well	2-41/75	0	2585 m	Taiyuan	16,161.60	7436.767	0.09	6515.744	31.85
Yi 10-1-26 Well	2-41/75	45	2585 m	Taiyuan	9153.41	4227.212	0.08	3655.608	20.80
Yi 10-1-26 Well	2-41/75	90	2585 m	Taiyuan	10,632.05	5003.672	0.06	4049.611	28.14
Yi 10-1-26 Well	2-68/75	0	2590 m	Taiyuan	10,565.45	5129.673	0.03	3745.309	34.63
Yi 10-1-26 Well	2-68/75	45	2590 m	Taiyuan	16,216.33	6774.773	0.20	8914.503	38.95
Yi 10-1-26 Well	2-68/75	90	2590 m	Taiyuan	12,497.17	5490.984	0.14	5753.312	34.82
Yi 76 Well	2-54/55	0	1872 m	Box 8	8414.54	3330.482	0.26	5923.928	26.04
Yi 76 Well	2-54/55	45	1872 m	Box 8	8023.51	3819.324	0.05	2974.208	34.73
Yi 76 Well	2-54/55	90	1872 m	Box 8	10,245.28	5072.907	0.01	3483.396	34.02
Yi 76 Well	4-2/59	0	1923 m	Shan 1	11,596.78	5761.990	0.006	3915.057	38.88
Yi 76 Well	4-2/59	45	1923 m	Shan 1	9289.83	4390.623	0.06	3502.300	30.15
Yi 76 Well	4-2/59	90	1923 m	Shan 1	18,535.96	8905.547	0.04	6726.130	47.47
Yi 76 Well	5-23/88	0	1928 m	Shan 1	27,823.17	13,535.175	0.03	9820.613	75.48
Yi 76 Well	5-23/88	45	1928 m	Shan 1	31,847.76	15,012.575	0.06	12,082.848	67.52
Yi 76 Well	5-23/88	90	1928 m	Shan 1	27,406.86	13,236.828	0.035	9828.543	92.62

Figure A1. A schematic representation of a standard rock sample and a processed rock sample is provided.

References

1. Qun, L.E.I.; Yun, X.U.; Bo, C.A.I.; Baoshan, G.; Xin, W.; Guoqiang, B.I.; Hui, L.I.; Shuai, L.I.; Bin, D.; Haifeng, F.U.; et al. Progress and prospects of horizontal well fracturing technology for shale oil and gas reservoirs. *Pet. Explor. Dev.* **2022**, *49*, 191–199.
2. Barati, R.; Liang, J. A review of fracturing fluid systems used for hydraulic fracturing of oil and gas wells. *J. Appl. Polym. Sci.* **2014**, *131*, e40735. [CrossRef]
3. Qi, E.; Xiong, F.; Cao, Z.; Zhang, Y.; Xue, Y.; Zhang, Z.; Ji, M. Simulation of Gas Fracturing in Reservoirs Based on a Coupled Thermo-Hydro-Mechanical-Damage Model. *Appl. Sci.* **2024**, *14*, 1763. [CrossRef]
4. Li, D.; Li, N.; Jia, J.; Yu, H.; Fan, Q.; Wang, L.; Mohsen, A. Development status and research recommendations for thermal extraction technology in deep hot dry rock reservoirs. *Deep. Undergr. Sci. Eng.* **2024**, *in press*. [CrossRef]
5. Yan, W.; Wang, C.; Yin, S.; Wen, Z.; Zheng, J.; Fu, X.; Feng, Z.; Zhang, Z.; Zhu, J. A log-based method for fine-scale evaluation of lithofacies and its applications to the Gulong shale in the Songliao Basin, Northeast China. *Energy Geosci.* **2024**, *5*, 100291. [CrossRef]
6. Ezazi, M.; Ghorbani, E.; Shafiei, A.; Teshnizi, E.S.; O'kelly, B.C. Laboratory Hydraulic Tensile Strength Correlation with Strength-Based Brittleness Indices for Carbonate Reservoirs. *Geosciences* **2024**, *14*, 52. [CrossRef]
7. Li, X.; He, M.; Huang, X.; Wu, K.; Zuo, X.; Xue, J.; Lu, J. Fracture extension behavior and micro-mechanical damage mechanism under different CO2 fracturing methods in continental shale reservoirs. *Fuel* **2024**, *365*, 131144. [CrossRef]
8. Wang, L.; Yu, F.; Shi, J.; Peng, J.; Zhao, W.; Liu, Y.; Yan, J. Study on engineering geological characteristics of southwest shale oil based on nuclear magnetic resonance imbibition flooding technology. *Acta Geophys.* **2024**, 1–15. [CrossRef]
9. Mukhopadhyay, P. Advances in Well Logging Techniques for Shale Reservoirs Exploration. In *Unconventional Shale Gas Exploration and Exploitation: Current Trends in Shale Gas Exploitation*; Springer International Publishing: Cham, Switzerland, 2024; pp. 31–47.
10. Yuan, J.L.; Deng, J.G.; Zhang, D.Y.; Li, D.H.; Yan, W.; Chen, C.G.; Cheng, L.J.; Chen, Z.J. Hydraulic fracturing tendency ecaluation of shale-gas reservoirs. *Acta Pet. Sin.* **2013**, *34*, 523–527.
11. Zhu, G.Z.; He, C.L.; Fan, J.Y. Log Evaluation Method for Gas Bearing and Hydraulic fracturing tendency of deep Shale Gas Reservoirs in Southern Sichuan. *Well Logging Technol.* **2022**, *46*, 433–438.
12. Chen, C.; Lei, Z.D.; Fang, M.J.; Qi, Y. Tight Sandstone Reservoir Compressibility Evaluation and Limit Parameter Fracturing Technology. *Sci. Technol. Eng.* **2022**, *22*, 6400–6407.
13. Zhao, J.Z.; Xu, W.J.; Li, Y.M.; Hu, J.Y.; Li, J.Q. A new method for evaluating the compressibility of shale-gas reservoirs. *Nat. Gas Geosci.* **2015**, *26*, 1165–1172.
14. Xiao, J.F.; Hu, P.J.; Han, L.X. Mechanical Properties and Compressibility Evaluation of Qiongzhusi shale in Weiyuan Area in Southern Sichuan. *Drill. Prod. Technol.* **2022**, *45*, 61–66.

15. Sun, Y.H.; Wang, F.; Wu, X.; Duan, Z.X.; Han, Z.X. CT scan-based quantitative characterization and hydraulic fracturing tendency evaluation of fractures in shale reservoirs. *Prog. Geophys.* **2023**, *38*, 2147–2159.
16. Chen, J.B.; Wei, B.; Xie, Q.; Wang, H.Q.; Li, T.T.; Wang, H. Multi-fracture simulation of shale horizontal wells based on extended finite element method. *Appl. Math. Mech.* **2016**, *37*, 73–83.
17. Wang, L.; Yang, J.; Peng, J.L.; Chen, G.; Han, H.; Zhang, X. Experimental Evaluation on Compressibility of Shale Oil Reservoir in Da'anzhai Section in Central Sichuan Area. *Drill. Prod. Technol.* **2023**, *46*, 163–168.
18. Sun, J.; Han, Z.; Qin, R.; Zhang, J. Log evaluation method of fracturing performance in tight gas reservoir. *Acta Pet. Sin.* **2015**, *36*, 74–80.
19. Zhang, C.; Xia, F.G.; Xia, Y.Q.; Zhou, X.L. Comprehensive Evaluation of Hydraulic fracturing tendency of Tight Sandstone Reservoirs Based on Analytic Hierarchy Process. *Drill. Prod. Technol.* **2021**, *44*, 61–64.
20. Zhai, W.B.; Li, J.; Zhou, Y.C.; Liu, G.H.; Huang, T.; Song, X.F. New evaluation method of shale reservoir hydraulic fracturing tendency based on logging data. *Lithol. Reserv.* **2018**, *30*, 112–123.
21. Ren, L.; Li, Y.B.; Peng, S.R.; Zhao, C.N.; Wu, J.F.; Li, Z.X. Predicting economic benefit of deep shale gas fracturing prediction based on comprehensive hydraulic fracturing tendency. *Oil Drill. Prod. Technol.* **2023**, *45*, 229–236.
22. Longinos, S.N.; Tuleugaliyev, M.; Hazlett, R. Influence of subsurface temperature on cryogenic fracturing efficacy of granite rocks from Kazakhstan. *Geothermics* **2024**, *118*, 102919. [CrossRef]
23. Tuzingila, R.M.; Kong, L.; Kasongo, R.K. A review on experimental techniques and their applications in the effects of mineral content on geomechanical properties of reservoir shale rock. *Rock Mech. Bull.* **2024**, *3*, 100110. [CrossRef]
24. Lou, Y.S.; Jing, Y.Q. *Rock Mechanics and Petroleum Engineering*; Petroleum Industry Press: Beijing, China, 2006.
25. Salah, M.; Ibrahim Mohamed, M.; Ibrahim, M.; Mazher, I.; Pieprzica, C. A newly developed approach to evaluate rock brittleness and hydraulic fracturing tendency for hydraulic fracturing optimization in shale gas. In Proceedings of the SPE Western Regional Meeting, San Jose, CA, USA, 23–26 April 2019.
26. Ghadimipour, A.; Perumalla, S.; Chakrabarti, P.; Ben Boudiaf, M.; Saha, S. De-Risking the Full Development Cycle of Tight Naturally Fractured Prospects by Integration of Advanced GeoMechanical and Natural Fracture Characterization: A North African Perspective. In Proceedings of the International Petroleum Technology Conference, Dhahran, Saudi Arabia, 12–14 February 2024.
27. Yao, T.; Qian, L.; Mo, Z.; Gao, Y.; Zhang, J.; Zhang, R.; Hu, Q.; Xing, X. A new brittleness index based on crack characteristic stress and its engineering applications. *Eng. Geol.* **2024**, *330*, 107411. [CrossRef]
28. Liang, W.; Wang, J.; Leung, C.; Goh, S.; Sang, S. Opportunities and challenges for gas coproduction from coal measure gas reservoirs with coal-shale-tight sandstone layers: A review. *Deep. Undergr. Sci. Eng.* **2024**, *in press*. [CrossRef]
29. Jiao, W.; Huang, Y.; Zhang, H.; Zhang, Y.; Zhao, D.; Wen, L.; Guo, P.; Zhang, J. Characteristics of Typical Shale Reservoir Development and Its Gas-Bearing Influencing Factors. *Chem. Technol. Fuels Oils* **2024**, *60*, 132–141. [CrossRef]
30. Tang, X.; Zhu, H.; Zhao, P.; Zeng, B.; Zhao, M.; Dusseault, M.B.; McLennan, J.D. A numerical study of complex fractures propagation path in naturally fractured gas shale: Reorientation, deflection and convergence. *Gas Sci. Eng.* **2024**, *121*, 205186. [CrossRef]
31. Luo, T.; Wang, J.; Chen, L.; Sun, C.; Liu, Q.; Wang, F. Quantitative characterization of the brittleness of deep shales by integrating mineral content, elastic parameters, in situ stress conditions and logging analysis. *Int. J. Coal Sci. Technol.* **2024**, *11*, 10. [CrossRef]
32. Gong, Y.; El-Monier, I.; Mehana, M. Machine Learning and Data Fusion Approach for Elastic Rock Properties Estimation and Fracturability Evaluation. *Energy AI* **2024**, *16*, 100335. [CrossRef]
33. Blake, O.O.; Ramsook, R.; Faulkner, D.R.; Iyare, U.C. Relationship Between the Static and Dynamic Bulk Moduli of Argillites. *Pure Appl. Geophys.* **2021**, *178*, 1339–1354. [CrossRef]
34. Wang, H.Q.; Chen, J.B.; Zhang, J.; Xie, Q.; Wei, B.; Zhao, Y.R. A New Method of Hydraulic fracturing tendency Evaluation of Shale Gas Reservoir Based on Weight Allocation. *Pet. Drill. Tech.* **2016**, *44*, 88–94.
35. Li, Y.; Ding, W.; Han, J.; Chen, X.; Huang, C.; Li, J.; Ding, S. Quantitative Prediction of the Development and Opening Sequence of Fractures in an Ultradeep Carbonate Reservoir: A Case Study of the Middle Ordovician in the Shunnan Area, Tarim Basin, China. *SPE J.* **2024**, *29*, 3091–3117. [CrossRef]
36. Zhou, Z.-L.; Hou, Z.-K.; Guo, Y.-T.; Zhao, H.; Wang, D.; Qiu, G.-Z.; Guo, W.-H. Experimental study of hydraulic fracturing for deep shale reservoir. *Eng. Fract. Mech.* **2024**, *in press*. [CrossRef]
37. Xia, X.; Wu, Z.; Song, H.; Wang, W.; Cui, H.; Tang, M. Numerical study of hydraulic fracturing on single-hole shale under fluid–solid coupling. *Géoméch. Geophys. Geo-Energy Geo-Resources* **2024**, *10*, 23. [CrossRef]
38. Chen, J.G.; Deng, J.G.; Yuan, J.L.; Yan, W.; Wei, B.H.; Tan, Q. Determination of fracture toughness of modes I and II of shale formation. *Rock Mech. Eng.* **2015**, *34*, 1101–1105.
39. Zeeman, E.C. Catastrophe theory. *Sci. Am.* **1976**, *234*, 65–83. [CrossRef]
40. Graf, W.L. Catastrophe theory as a model for change in fluvial systems. In *Adjustments of the Fluvial System*; Routledge: London, UK, 2020; pp. 13–32.
41. Pan, R.; Liu, J.; Cheng, H.; Fan, H. Study on the Vertical Stability of Drilling Wellbore under Optimized Constraints. *Appl. Sci.* **2024**, *14*, 2317. [CrossRef]
42. Karman, A.; Pawłowski, M. Circular economy competitiveness evaluation model based on the catastrophe progression method. *J. Environ. Manag.* **2021**, *303*, 114223. [CrossRef] [PubMed]
43. Jiang, X. Risk Assessment of Maritime Traffic Safety Based on Catastrophe Theory. *Front. Soc. Sci. Technol.* **2023**, *5*, 80–84.

44. Cheng, H.; Yang, X.; Lan, Y. Investigating rock mutation characteristics and damage state warning model based on energy conversion. *Energy Sci. Eng.* **2024**, *12*, 1221–1232. [CrossRef]
45. Teng, H.; Qian, Y.; Lan, Y.; Cui, W. Swallowtail-type diffraction catastrophe beams. *Opt. Express* **2021**, *29*, 3786–3794. [CrossRef] [PubMed]
46. Teng, H.; Hu, J.; Cai, Y.; Lan, Y.; Qian, Y. Caustics and wavefront of Swallowtail-Gauss catastrophe beams. *Results Phys.* **2022**, *42*, 105991. [CrossRef]
47. Faeq, I.R.; Abdalrahman, S.O. The Stability and Catastrophic Behavior of Finite Periodic Solutions in Non-Linear Differential Equations. *Tikrit J. Pure Sci.* **2023**, *28*, 146–152. [CrossRef]
48. Wei, X.; Wang, X.; Chen, T.; Ding, Z.; Wu, X. Comparison of the Fold and Cusp Catastrophe Models for Tensile Cracking and Sliding Rockburst. *Math. Probl. Eng.* **2021**, *2021*, 1–10. [CrossRef]
49. Zhai, W.; Li, J.; Zhou, Y. Application of catastrophe theory to hydraulic fracturing tendency evaluation of deep shale reservoir. *Arab. J. Geosci.* **2019**, *12*, 76–79. [CrossRef]
50. Liang, G.L.; Xu, W.Y.; He, Y.Z.; Zhao, Y. Application of catastrophe progression method to comprehensive evaluation of slope stability. *Rock Soil Mech.* **2008**, *29*, 1895–1899.